

Electro-Mechanical Response of Nematic Elastomers: an Introduction

Antonio DeSimone*

April 11, 2011

**Mechanics and Electrodynamics of Magneto-
and Electro-Elastic Materials,
R.W. Ogden and D. Steigmann eds.,
CISM Courses and Lectures, vol. 527, pp. 231–266.**

Abstract

We review in these lecture notes some of our recent work on modelling the response of nematic elastomers to applied mechanical loads and/or to electric fields, both in the static and in the dynamic regime. Our aim is to compare theoretical results based on mathematical analysis and on numerical simulations with the available experimental evidence, in order to examine critically the various recent accomplishments, and some challenging problems that remain open. Nematic elastomers combine the electro-optical properties and rotational degrees of freedom of nematic liquid crystals with the mechanical properties and translational degrees of freedom of entropic rubbery solids. The rich behavior they exhibit, the interesting applications they seem to make possible, the breadth and depth of recent breakthroughs at the experimental, theoretical, and computational level make nematic elastomers an exciting model system for advanced research in mechanics.

Keywords: Liquid Crystals, Polymers, Nematic Elastomers, Anisotropic Dielectrics, Domain Patterns, Nonlinear Elasticity, Electro-Mechanical Coupling, Nonconvex Problems in the Calculus of Variations, Relaxation, Analysis and Numerical Simulation of Microstructures.

AMS Subject Classification: 74N15, 74B20, 49J45.

*SISSA–International School for Advanced Studies, Via Bonomea 265, 34136 Trieste, ITALY

Contents

1	Introduction	3
2	Molecular structure and macroscopic response	3
3	Warm-up in finite dimensions	7
4	Elastic energy densities for nematic elastomers	10
5	Material instabilities	14
6	Effective energy: coarse-graining and quasi-convexification	19
7	Dynamics under an applied electric field	26
8	Comparison with key experimental results	29
8.1	Stretch	32
8.2	Shear	33
8.3	Electric field applied to a free-standing film	35
8.4	Discussion	35
9	Appendix: alignment energies	37

1 Introduction

In these lecture notes we focus on the electro-mechanical behavior of *one* specific material: nematic elastomers. It is a new material, so our understanding of it is still incomplete. Among its distinguishing features are large spontaneous deformations, actuation by many different means including electric fields, and mechanical compliance. This makes it suitable for fast soft actuators and, in particular, for new applications such as artificial muscles, which are currently of great technological interest. The reader is referred to the monograph [30] for a detailed account of the chemistry and physics of nematic elastomers, and for an extensive list of references.

The mechanism for electro-mechanical coupling is the anisotropy of dielectric constants, as it is typical for liquid crystals. Nematic Liquid Crystal Displays (LCDs), which represent one of the biggest market arenas for technological devices based on electro-mechanical coupling, exploit precisely this mechanism. Indeed, a localized applied voltage is able to change the local orientation of nematic molecules, which in turn results in a change of optical properties: the material can change from being transparent to opaque when sandwiched between crossed polarizers, giving rise to a very reliable optical micro-shutter. Individual pixels of LCDs are realized in this fashion. We notice that the mechanism for electro-mechanical coupling based on dielectric anisotropy is different from those based on either permanent or induced polarization, which occur in ferroelectric and piezoelectric materials, respectively. Indeed, nematic elastomers are neither ferroelectric nor piezoelectric.

Nematic elastomers provide a counterpart in the world of rubbery solids to nematic liquid crystals. Thanks to the coupling with nematic degrees of freedom, their entropic elasticity can be activated by temperature changes (similarly to what happens in shape-memory alloys SMAs), electric fields (like in electro-active polymers EAPs), or by irradiation with UV light. The lessons one can learn by studying this fascinating model material may provide very useful insight on the behavior of many other interesting systems.

2 Molecular structure and macroscopic response

Nematic elastomers consist of cross-linked networks of polymeric chains containing nematic mesogens. The three main chemical constituents of this assembly are a polymer backbone, nematic mesogens, and cross-linkers.

The *polymer backbone* results from the repeat of monomers containing

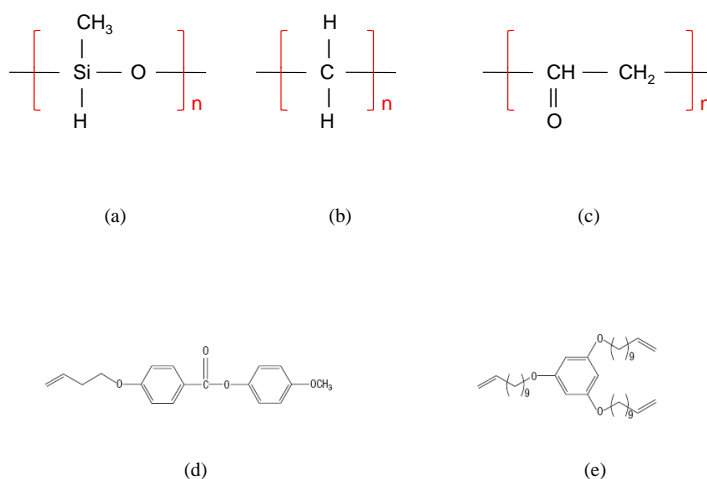


Figure 1: Basic chemistry of nematic elastomers. On the top row, some typical polymer backbones: methyl-siloxane, an example of polysiloxane (a), a $(\text{CH}_2)_n$ chain (b), and polyacrylate (c). On the bottom row, a bi-phenyl side-chain nematic mesogen (d) and a tri-functional cross-linker (e).

tetra-valent atoms, such as Carbon (C) or Silicon (Si), that are able to form long and flexible chains. In these geometries, two bonds are used to construct a connected chain, while two more bonds are free and available for attachment of side units (see Figure 1).

Nematic mesogens are rigid rod-like molecules containing benzenic rings. They are responsible for the establishment of nematic order at sufficiently low temperatures. The isotropic-to-nematic transition is a phase transformation determined by the alignment of the nematic mesogens, and accompanied by a change of the optical properties of the system (which becomes anisotropic). At the same time, the material tends to become transparent. Nematic mesogens can either be part of the backbone (main-chain nematic elastomer) or be attached sideways (side-chain nematic elastomers). The possibility of attachment typically comes from the presence of a double carbon bond $\text{C}=\text{C}$ which can open up into $-\text{C}-\text{C}-$ leaving the unsaturated ends free for bonding.

Depending on whether the $\text{C}=\text{C}$ unit is at one end or in the central part of the nematic mesogen, this will orient parallel or perpendicular to the backbone giving rise to prolate or oblate structures. When the isotropic-

to-nematic phase transition takes place, the alignment of nematic mesogens causes a distortion of the polymer backbone to which they are attached. We will be mostly concerned with the prolate case, in which the polymer chains tend to elongate along the direction of alignment of the nematic mesogens.

Cross-linkers are flexible chains containing double C=C bonds at both ends. Hence they are able to attach to two distinct polymer chains, connecting them. This is what turns an ensemble of disjoint polymer chains (a polymeric liquid) into a percolating network able to transmit static shear stresses (an elastomer, or rubbery solid). The combination of polymer backbone, nematic mesogens, and cross-linkers leads to a system in which the orientational degrees of freedom and the associated optical-elastic properties typical of nematic liquid crystals (dielectric anisotropy, Frank curvature elasticity associated with spatial variations of nematic order) appear in combination with the mechanical properties and the translational degrees of freedom exhibited by an elastic solid (deformation gradients, rubber elasticity, shear moduli).

The coupling between nematic orientational order and rubber entropic elasticity has profound consequences. The alignment of nematic mesogens in a neighborhood of a point x along an average direction $\pm\mathbf{n}(x)$, where \mathbf{n} is a unit vector field called *nematic director*, induces a spontaneous distortion of the polymer chains described by

$$\mathbf{V}_{\mathbf{n}} = a^{1/3}\mathbf{N} + a^{-1/6}(\mathbf{I} - \mathbf{N}) \quad (2.1)$$

where $a > 1$ (prolate case), \mathbf{I} is the identity, and

$$\mathbf{N} = \mathbf{n} \otimes \mathbf{n}. \quad (2.2)$$

Here $\mathbf{a} \otimes \mathbf{b}$ denotes the tensor product of the vectors \mathbf{a} and \mathbf{b} with components $(\mathbf{a} \otimes \mathbf{b})_{ij} = a_i b_j$. Tensor \mathbf{N} is closely related to de Gennes's order tensor \mathbf{Q} . Here we are using the framework of Frank-type theories, in which order is constrained to be uniaxial and the degree of order is fixed. Then, one has $\mathbf{Q} = s(\mathbf{N} - (1/3)\mathbf{I})$, with $s > 0$ constant, and the descriptions of nematic order in terms of either \mathbf{Q} or \mathbf{N} are equivalent. The material parameter a , which in the oblate case is smaller than one, gives the amount of spontaneous elongation along \mathbf{n} accompanying the isotropic-to-nematic phase transformation. It is a combined measure of the degree of order and of the strength of the nematic-elastic coupling, and it is in principle a function of temperature. We will ignore this, as we will be working at a fixed, constant temperature, well below the isotropic-to-nematic transition temperature T_{IN} . Tensor $\mathbf{V}_{\mathbf{n}}$ represents a volume-preserving uniaxial stretch along the *current* direction of the director \mathbf{n} .

The spontaneous distortion (2.1) can be very large (up to 300% in some main-chain elastomers) and it is easily observable when the temperature of the elastomer is lowered below T_{IN} starting from a temperature above T_{IN} (at which the material behaves like a standard rubber). Working at fixed $T < T_{IN}$, one way of observing (2.1) is to apply an electric field to a mechanically unconstrained sample (e.g., a nematic gel surrounded by silicon oil, inside a capacitor with transparent electrodes). As it is well known from ordinary nematic liquids, due to the anisotropy of the dielectric tensor (we assume here that the material has positive dielectric anisotropy: $\varepsilon_a > 0$), a sufficiently strong applied voltage tends to align the director with the electric field \mathbf{E} , i.e., $\mathbf{n} = \pm \mathbf{E}/|\mathbf{E}|$. The quantitative details of this coupling will be described later, see Section 7. Suffice it to say here that by rotating the applied field one may induce rotations of \mathbf{n} and observe the macroscopic shape changes of the sample accompanying this process. Also, simultaneous birefringence measurements can be used to determine directly the dependence of \mathbf{n} on the applied electric field. It turns out that the correlation between observed deformations and measured \mathbf{n} follows equation (2.1) to a remarkable level of accuracy, see [20].

A more subtle consequence of (2.1) emerges in stretching experiments in the absence of applied electric fields. Again, the temperature is fixed at a constant value below T_{IN} . The sample is prepared so that the director is spatially uniform, say \mathbf{n} aligned with \mathbf{e}_3 , the third unit vector of the canonical basis, and its initial state is the natural one corresponding to $\mathbf{n} = \mathbf{e}_3$. This means that polymer chains are elongated along the direction of \mathbf{e}_3 , with stretch $a^{1/3} > 1$ along \mathbf{e}_3 with respect to the reference configuration. Imagine now that the sample, a thin film with thickness direction parallel to \mathbf{e}_1 , is stretched along \mathbf{e}_2 , with rigid clamps applied on the two edges perpendicular to \mathbf{e}_2 . Experiments show that the force–stretch diagram is unusually soft, with an extended flat plateau following a small region of initially hard response. We will refer in what follows to the idealized case in which this initially hard regime is not present as the *ideally soft* case. The interpretation of this unusual softness is that the sample accommodates the externally imposed deformations by reorienting the director along the direction of maximal stretch, hence storing less elastic energy. This is confirmed by optical microscopy under crossed polarizers, which reveals a texture of opaque and transparent bands parallel to \mathbf{e}_2 . The existence of this optical contrast shows that the director reorientation process occurs in a spatially nonuniform manner (*stripe-domain patterns*); in view of the coupling implied by (2.1), oscillating shears are triggered by the oscillations of the nematic director. This means that nematic elastomers exhibit material instabilities (co-operative elastic shear banding, which is fully reversible, see Sections 5

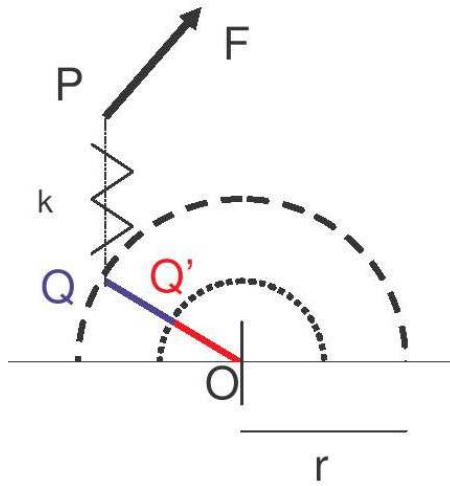


Figure 2: A finite-dimensional model system.

and 6) as a consequence of the spontaneous distortion (2.1) accompanying the symmetry breaking transformation from the high temperature isotropic phase to the low temperature nematic phase.

3 Warm-up in finite dimensions

Consider the following model mechanical system, lying in the plane $\{\mathbf{0}, \mathbf{e}_1, \mathbf{e}_2\}$. It is made of two rigid links \mathbf{OQ}' , and $\mathbf{Q}'\mathbf{Q}$, each of length $r/2 > 0$, and of an extensible spring \mathbf{QP} with stiffness $k > 0$. There are frictionless joints in \mathbf{O} , \mathbf{Q}' , and \mathbf{Q} , so that \mathbf{O} is fixed and only relative rotations are allowed in \mathbf{Q}' and \mathbf{Q} . A force $\mathbf{F} = F_1\mathbf{e}_1 + F_2\mathbf{e}_2$ acts on the free end \mathbf{P} , and all points are constrained to lie in the half-plane $x_2 \geq 0$.

We are interested in the following problem. Given an arbitrary force \mathbf{F}

with $\mathbf{F} \cdot \mathbf{e}_2 \geq 0$, find the configurations of the system minimizing its energy

$$\mathcal{E}(\mathbf{P}, \mathbf{Q}) = \frac{k}{2} |\mathbf{P} - \mathbf{Q}|^2 - \mathbf{F} \cdot \mathbf{P}. \quad (3.1)$$

Once this problem is solved for every \mathbf{F} , we can imagine to fix the direction of \mathbf{F} , say, $\mathbf{F} = F\mathbf{e}$ and to vary its intensity F . By plotting the component along \mathbf{e} of the solution $\mathbf{P} - \mathbf{O}$ of the minimization problem against the value F of the corresponding force we may obtain a force-stretch diagram summarizing the essentials of the mechanical response of the system to the prescribed applied loads.

It is interesting to notice that, since \mathbf{OQ}' and $\mathbf{Q}'\mathbf{Q}$ are inextensible, the configuration of the whole system is uniquely identified by the position of points \mathbf{P} and \mathbf{Q} . Point \mathbf{Q} is, however, an internal variable in the sense that no external force is directly applied to it. Moreover, in view of the constraints present on the system, the set of admissible positions for point \mathbf{Q} is

$$\mathcal{A} := \{\mathbf{Q} \in \mathbb{R}^2 : |\mathbf{Q} - \mathbf{O}| \leq r, \mathbf{Q} \cdot \mathbf{e}_2 \geq 0\} \quad (3.2)$$

We may obtain the solution to the problem above in two steps. First we minimize out the internal variable \mathbf{Q} . Indeed

$$\min_{\mathbf{P}, \mathbf{Q}} \mathcal{E}(\mathbf{P}, \mathbf{Q}) = \min_{\mathbf{P}} \left(\min_{\mathbf{Q}} \frac{k}{2} |\mathbf{P} - \mathbf{Q}|^2 - \mathbf{F} \cdot \mathbf{P} \right). \quad (3.3)$$

We set

$$\mathcal{E}_{\text{eff}}(\mathbf{P}) = \min_{\mathbf{Q}} \frac{k}{2} |\mathbf{P} - \mathbf{Q}|^2 = \frac{k}{2} |\mathbf{P} - \mathbf{Q}_{\mathbf{P}}|^2 \quad (3.4)$$

where $\mathbf{Q}_{\mathbf{P}}$ is the orthogonal projection of \mathbf{P} onto the closed convex set \mathcal{A} . Notice that $\mathbf{Q}_{\mathbf{P}}$ coincides with \mathbf{P} if $\mathbf{P} \in \mathcal{A}$.

Granted (3.3) and (3.4), we can perform the second step in our minimization problem

$$\min_{\mathbf{P}, \mathbf{Q}} E(\mathbf{P}, \mathbf{Q}) = \min_{\mathbf{P}} (\mathcal{E}_{\text{eff}}(\mathbf{P}) - \mathbf{F} \cdot \mathbf{P}). \quad (3.5)$$

If we consider a stretching experiment starting from $\mathbf{Q} = \mathbf{O}$, an equilibrium configuration under zero force, we obtain a zero force response with \mathbf{Q} moving along a segment parallel to \mathbf{e} until $\mathbf{Q} - \mathbf{O} = r\mathbf{e}$. The force response to further extension is linear, given by $k(|\mathbf{P} - \mathbf{O}| - r)$. In other words, we can obtain the force response by differentiating \mathcal{E}_{eff} .

In spite of its simplicity, the model finite-dimensional system described in this section provides some interesting guidance for our future developments. For example, it shows that in spite of non-uniqueness of the minimal energy configuration of the two rigid links in the determination of (3.4) (notice that

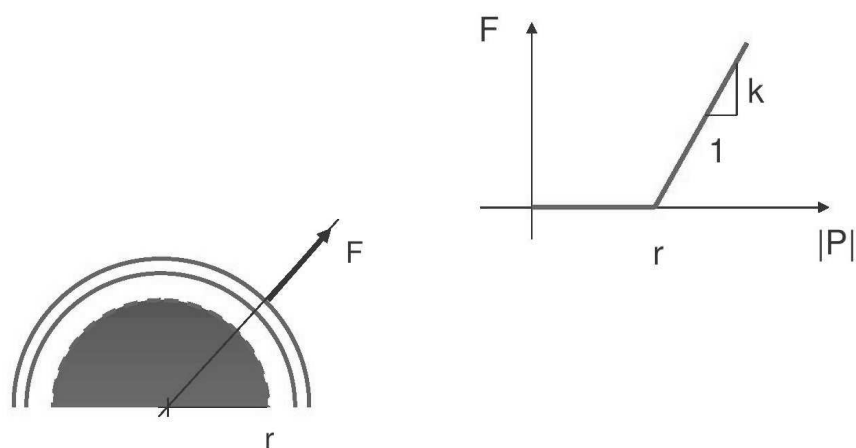


Figure 3: Level curves of the energy (left) and the force response (right) of the finite-dimensional model system.

\mathbf{Q}' is not uniquely defined by $\mathbf{Q}_{\mathbf{P}}$ in (3.5) if $|\mathbf{P} - \mathbf{O}| < r$, the effective energy itself, \mathcal{E}_{eff} , and (hence) the force-stretch diagram are unique. Moreover, the example raises the question of dynamic accessibility of the energy-minimizing states. Indeed, if after having reached the linear regime in the extension experiment we reversed the sign of the force, a buckling instability would occur at $|\mathbf{Q} - \mathbf{O}| = r$. Following one of the buckling branches one can return to the initial configuration $\mathbf{Q} = \mathbf{O}$. Following the symmetric path we would hit the constraint $x_2 \geq 0$ preventing us from reaching $\mathbf{Q} = \mathbf{O}$.

The notion of effective energy will appear in what follows in two different circumstances, in particular in Section 6. One is the energy density $W_{\text{eff}}(\mathbf{F})$ arising from optimizing over the nematic degrees of freedom the energy density $W(\mathbf{F}, \mathbf{n})$, at fixed deformation gradient \mathbf{F} . Another one is the coarse-graining of the energy W_{eff} over elastic degrees of freedom oscillating at fine length-scales (microstructures), in order to compute its quasi-convex envelope $W_{\text{eff}}^{\text{qc}}$.

4 Elastic energy densities for nematic elastomers

This section is mostly based on [15], to which the reader is referred for further details. We will denote by $\mathbf{F} = \nabla \mathbf{y}$ the gradient of the deformation with respect to the reference configuration, chosen as the one the sample would exhibit if stress-free in the high-temperature isotropic state. Moreover, we denote by $J = \det \mathbf{F}$ the determinant of the deformation gradient \mathbf{F} . In our discussion we focus on the most basic (and fundamental) expression for the elastic energy density stored by a nematic elastomer. This is based on the trace formula of Bladon, Terentjev, and Warner [3] which, after a change of variables first proposed in [11], becomes

$$W(\mathbf{F}, \mathbf{N}) = \frac{1}{2} \mu \mathbf{B}^e \cdot \mathbf{I}, \quad \det \mathbf{B}^e = J^2 = 1, \quad (4.1)$$

$$\mathbf{B}^e(\mathbf{F}, \mathbf{N}) = \mathbf{B} \mathbf{L}^{-1} = \mathbf{F} \mathbf{F}^T \mathbf{L}^{-1}(\mathbf{N}),$$

where

$$\mathbf{L}(\mathbf{N}) := a^{\frac{2}{3}} \mathbf{N} + a^{-\frac{1}{3}} (\mathbf{I} - \mathbf{N}) = \mathbf{V}_{\mathbf{n}}^2 \quad (4.2)$$

and $\mathbf{V}_{\mathbf{n}}$ is the spontaneous stretch defined in (2.1). The second line in (4.1) emphasizes that, according to the trace formula, the part of the deformation responsible for storage of elastic energy (the elastic part in a multiplicative decomposition, in the same spirit of the Kroener-Lee multiplicative decomposition in finite plasticity) is $\mathbf{B}^e = \mathbf{B} \mathbf{L}^{-1}$. To the best of our knowledge,

this seemingly obvious observation has not been made before [15], in spite of the fact that it has profound implications.

Proposition 1 in Section 9 shows that, given an arbitrary current orientation of the nematic director \mathbf{N} , (4.1) is minimized at the energy level $\frac{3}{2}\mu$, which is independent of \mathbf{N} , by any deformation p_0 with $\nabla p_0 \nabla p_0^T = \mathbf{L}(\mathbf{N})$. By the polar decomposition theorem, ∇p_0 is then of the form

$$\nabla p_0 = \mathbf{L}^{\frac{1}{2}}(\mathbf{N})\mathbf{Q}, \quad (4.3)$$

where \mathbf{Q} is an arbitrary rotation. Every pair $(\nabla p_0, \mathbf{N})$ is a natural, stress-free state for a material described by the energy density W above.

Formula (4.1) lends itself to easy and useful generalizations. Expressions for the energy density, which are more suitable to study the regime of high stresses, can be obtained by replacing (4.1) with

$$W(\mathbf{F}, \mathbf{N}) = W_{iso}(\mathbf{B}^e(\mathbf{F}, \mathbf{N})) , \quad J = 1, \quad (4.4)$$

where one may choose for $W_{iso}(\mathbf{B}^e)$ any of the available functional forms used to model isotropic incompressible elastic materials, which have a strict global minimum at $\mathbf{B}^e = \mathbf{I}$. Formula (4.1) corresponds to the Neo-Hookean expression; a few other alternative examples are listed in [15]. We quote here, in particular, the Ogden form

$$\begin{aligned} & \sum_{i=1}^N a_i \operatorname{tr}(\mathbf{B}^e)^{\gamma_i/2} + \sum_{j=1}^M b_j \operatorname{tr}(\operatorname{cof} \mathbf{B}^e)^{\delta_j/2} = \\ & = \sum_{i=1}^N a_i (v_1^{\gamma_i} + v_2^{\gamma_i} + v_3^{\gamma_i}) + \sum_{j=1}^M b_j ((v_2 v_3)^{\delta_j} + (v_3 v_1)^{\delta_j} + (v_1 v_2)^{\delta_j}) \end{aligned}$$

where v_k denotes the k -th principal stretch, i.e., the square root of the k -th eigenvalue of \mathbf{B}^e .

Extensions of Formula (4.1) to the compressible case are also straightforward, by setting

$$\tilde{W}(\mathbf{F}, \mathbf{N}) = W_{iso}(\mathbf{B}_s^e(\mathbf{F}, \mathbf{N})) + W_{vol}(J), \quad \mathbf{B}_s^e = J^{-2/3} \mathbf{B}^e. \quad (4.5)$$

Here $W_{vol}(s)$ is a non-negative, strictly convex function which is finite only for $s > 0$, vanishes only at $s = 1$, and diverges to $+\infty$ as s tends to either 0 or $+\infty$. This modification leaves the energy-well structure unchanged, because the minimizers of (4.5) are clearly the same of (4.1). Since in what follows we will be only interested in the behavior of the energy in a neighborhood of a natural state, a quadratic expansion of W_{vol} may suffice leading to the following model expression for the compressible isotropic case

$$\tilde{W}(\mathbf{F}, \mathbf{N}) = \frac{1}{2}\mu \mathbf{B}_s \cdot \mathbf{L}^{-1}(\mathbf{N}) + \frac{1}{2}\kappa \left(\sqrt{\det \mathbf{B}} - 1 \right)^2. \quad (4.6)$$

Another important generalization is discussed in detail in [15], and it consists in adding some anisotropic corrections to the isotropic energies described above. The two most basic ones are given below. The first one is

$$\tilde{W}_\beta(\mathbf{F}, \mathbf{N}) = \frac{1}{2}\mu_\beta \mathbf{C}_s \cdot \mathbf{L}_a^{-1} + \tilde{W}(\mathbf{F}, \mathbf{N}), \quad (4.7)$$

where $\mathbf{C}_s := (\det \mathbf{C})^{-2/3} \mathbf{C}$ and

$$\mathbf{L}_a := \mathbf{L}(\mathbf{N}_a) = a^{\frac{2}{3}} \mathbf{N}_a + a^{-\frac{1}{3}}(\mathbf{I} - \mathbf{N}_a)$$

with $\mathbf{N}_a := \mathbf{n}_a \otimes \mathbf{n}_a$ and \mathbf{n}_a a unit vector along the axis of anisotropy in the reference configuration. The second model anisotropic expression is

$$\tilde{W}_\alpha(\mathbf{F}, \mathbf{N}) = \frac{1}{2}\mu_\alpha(1 - \mathbf{N} \cdot \mathbf{N}^*(\mathbf{F})) + \tilde{W}(\mathbf{F}, \mathbf{N}), \quad (4.8)$$

where

$$\mathbf{N}^* := \mathbf{n}^* \otimes \mathbf{n}^*, \quad \mathbf{n}^* = \mathbf{n}^*(\mathbf{F}) := \frac{\mathbf{F}\mathbf{n}_a}{|\mathbf{F}\mathbf{n}_a|}, \quad (4.9)$$

and \mathbf{n}^* gives the current orientation of the axis of anisotropy \mathbf{n}_a . A somewhat related model, based on the notion of nonlinear relative rotations has been proposed in [26].

Finally, we consider the analogues of the energy densities described above in the framework of a geometrically linear theory. These are derived in [15], by Taylor expansion. Assume that $a^{1/3} = 1 + \gamma$, with $0 < \gamma \ll 1$. We then have

$$\mathbf{L}^{-1}(\mathbf{N}) = \mathbf{I} - 3\gamma(\mathbf{N} - \frac{1}{3}\mathbf{I}) + 3\gamma^2\mathbf{N}. \quad (4.10)$$

Assume moreover that $\mathbf{F} = \mathbf{I} + \nabla \mathbf{u}$, where $\mathbf{u}(x) = \mathbf{y}(x) - x$ is the displacement, and $|\nabla \mathbf{u}| = \varepsilon \ll 1$. We then have $\mathbf{B} = \mathbf{I} + 2\mathbf{E} + o(\varepsilon^2)$, where \mathbf{E} is the symmetric part of the displacement gradient (linear strain), and

$$\begin{aligned} \mathbf{B}_s &= (\det(\mathbf{I} + 2\mathbf{E}))^{-\frac{1}{3}}(\mathbf{I} + 2\mathbf{E}) \\ &= \mathbf{I} + 2\mathbf{E}_d + \frac{2}{3}((\mathbf{E} \cdot \mathbf{E} + \frac{1}{3}(\text{tr}(\mathbf{E}))^2)\mathbf{I} - 2\text{tr}(\mathbf{E})\mathbf{E}) + o(\varepsilon^2), \end{aligned} \quad (4.11)$$

where \mathbf{E}_d is the deviatoric part of \mathbf{E} , see [15]. It follows from (4.10) and (4.11) that

$$\mathbf{B}_s \cdot \mathbf{L}^{-1} = 3 + 2(\mathbf{E}_d - \mathbf{E}_0(\mathbf{N})) \cdot (\mathbf{E}_d - \mathbf{E}_0(\mathbf{N})) + o(\varepsilon^2, \gamma^2, \varepsilon\gamma), \quad (4.12)$$

where

$$\mathbf{E}_0(\mathbf{n}) = \frac{3}{2}\gamma(\mathbf{n} \otimes \mathbf{n} - \frac{1}{3}\mathbf{I}) \quad (4.13)$$

represents the small strain counterpart of the spontaneous strain \mathbf{V}_n given in (2.1). Finally, we have that

$$(\sqrt{\det \mathbf{B}} - 1)^2 = (\text{tr } \mathbf{E})^2 + o(\varepsilon^2). \quad (4.14)$$

The calculations above show that, modulo additive constants, the small strain counterpart of \tilde{W} is given by the following expression

$$\tilde{\Phi}(\mathbf{E}, \mathbf{N}) = \mu |\mathbf{E}_d - \mathbf{E}_0(\mathbf{N})|^2 + \frac{1}{2} \kappa (\text{tr } \mathbf{E})^2. \quad (4.15)$$

The incompressible version is obtained by formally setting $\kappa = +\infty$, so that

$$\Phi(\mathbf{E}, \mathbf{N}) = \mu |\mathbf{E}_d - \mathbf{E}_0(\mathbf{N})|^2, \quad \text{tr } \mathbf{E} = \text{div } \mathbf{u} = 0. \quad (4.16)$$

It is worth comparing the expressions $\mathbf{B}^e = \mathbf{B}\mathbf{L}^{-1}(\mathbf{N})$ and $\mathbf{E}^e = \mathbf{E} - \mathbf{E}_0(\mathbf{N})$, which describe the relative deformation between the current one and the preferred one associated with \mathbf{N} . The first expression does this through the composition with an inverse, as it should be expected in nonlinear kinematics; the second one through a difference, as it is appropriate in linear kinematics. In both cases, it is only this relative deformation (the elastic part of the appropriate strain measure) that contributes to storage of elastic energy. A rigorous proof that (the quasiconvexification of) (4.16) gives the correct small-strain limit of (4.6) (in the sense of Gamma-convergence) is provided in [1].

The expansion of W_β works similarly, and one obtains

$$\tilde{\Phi}_\beta(\mathbf{E}, \mathbf{N}) = \tilde{\Phi}(\mathbf{E}, \mathbf{N}) + \mu_\beta |\mathbf{E}_d - \mathbf{E}_0(\mathbf{N}_a)|^2 \quad (4.17)$$

as the small strain counterpart of \tilde{W}_β . The small-strain approximation of \tilde{W}_α is instead more complicated, and we only report here a simplified expression valid in the regime where director rotations are large, while strains are small

$$\tilde{\Phi}_\alpha(\mathbf{E}, \mathbf{N}) = \tilde{\Phi}(\mathbf{E}, \mathbf{N}) + \frac{1}{2} \mu_\alpha (1 - \mathbf{N} \cdot \mathbf{N}_a), \quad (4.18)$$

where $\tilde{\Phi}$ is given in (4.15). This energy has been used in [20] to analyze the response of a free-standing film of a swollen nematic elastomer, to which an electric field is applied in order to drive the director away from its initial direction $\mathbf{n} = \mathbf{n}_a$. In the experiments, a finite critical field needs to be overcome in order to trigger director rotation. Measuring the equilibrium angle between \mathbf{n} and \mathbf{n}_a as a function of the applied electric field provides an experimental validation of (4.18) and a way of determining the value of the material parameter μ_α . It turns out that, when the field is removed, the director relaxes back to its preferred orientation \mathbf{n}_a . When $\mu_\alpha = 0$, the spring-back mechanism is suppressed and the critical field needed to start director reorientation is zero, see [20, Eq.(24)]. Interestingly, if one describes anisotropy using (4.17) instead of (4.18), the spring-back mechanism is suppressed.

5 Material instabilities

We choose a reference frame so that \mathbf{n}_a is along the third coordinate axis and set

$$\mathbf{n}(\theta) = \begin{bmatrix} 0 \\ \sin \theta \\ \cos \theta \end{bmatrix}, \quad \mathbf{n}_a = \begin{bmatrix} 0 \\ 0 \\ 1 \end{bmatrix}, \quad (5.1)$$

where θ is the angle between \mathbf{n} and \mathbf{n}_a . The state with $\theta = 0$ and $\mathbf{F} = \mathbf{L}_a^{1/2}$ is a global minimizer for all the energies introduced above. We are interested in the stability with respect to superposed shears of equilibrium states with $\theta = 0$, both in the initial configuration and in those obtained by (moderately) stretching the material in a direction perpendicular to \mathbf{n}_a . For this purpose, we consider the deformations

$$\mathbf{F}(\delta; \lambda) = \begin{bmatrix} a^{-1/6} & 0 & 0 \\ 0 & \lambda & \delta \\ 0 & 0 & a^{1/6}/\lambda \end{bmatrix} \quad (5.2)$$

with λ a fixed stretching parameter varying in a right neighborhood of $a^{-1/6}$. More precisely, we will take $\lambda \in [a^{-1/6}, a^{1/12})$.

By substituting $\mathbf{F}(\delta; \lambda)$ and $\mathbf{n}(\theta)$ in the various expressions of the energy, equations (4.6)–(4.8), we obtain three energies of the form $f(\delta, \theta; \lambda)$. In all cases $\partial f / \partial \delta$ and $\partial f / \partial \theta$ vanish at $\delta = \theta = 0$. Thus $\delta = \theta = 0$ is always an equilibrium configuration (this is easily seen by symmetry under $\pm \delta$ and $\pm \theta$) and we obtain expansions to second order of the following form

$$f(\delta, \theta; \lambda) = f(0, 0; \lambda) + \frac{1}{2} (G_{\delta\delta} \delta^2 + 2G_{\delta\theta} \delta\theta + G_{\theta\theta} \theta^2), \quad (5.3)$$

where

$$G_{\delta\delta}(\lambda) = \frac{\partial^2 f}{\partial \delta^2}(0, 0; \lambda), \quad G_{\delta\theta}(\lambda) = \frac{\partial^2 f}{\partial \delta \partial \theta}(0, 0; \lambda), \quad G_{\theta\theta}(\lambda) = \frac{\partial^2 f}{\partial \theta^2}(0, 0; \lambda). \quad (5.4)$$

The equilibrium value θ_0 of θ as a function of δ is obtained from

$$G_{\delta\theta} \delta + G_{\theta\theta} \theta = 0 \Rightarrow \theta_0(\delta) = -\frac{G_{\delta\theta}}{G_{\theta\theta}} \delta, \quad (5.5)$$

and substituting this into (5.3) we get

$$f(\delta, \theta_0(\delta); \lambda) - f(0, 0; \lambda) = \frac{1}{2} G(\lambda) \delta^2, \quad (5.6)$$

where we have set

$$G(\lambda) = \left(G_{\delta\delta} - \frac{G_{\delta\theta}^2}{G_{\theta\theta}} \right). \quad (5.7)$$

Depending on whether $G(\lambda) > 0$, $G(\lambda) = 0$, or $G(\lambda) < 0$, we have that the equilibrium state ($\delta = 0, \theta = 0$) is stable, neutrally stable, or unstable with respect to superposed shears. The special case $\lambda = a^{-\frac{1}{6}}$ reproduces de Gennes' analysis in [9]: simple shear from the natural state corresponding to $\mathbf{N} = \mathbf{N}_r$. Small shears superposed to large stretches have been considered also in [32], and the case of small shears superposed to large deformations arising in uniaxial extension experiments has been considered in [2].

We now compute $G(\lambda)$ for the three model energies \tilde{W} , \tilde{W}_β , \tilde{W}_α , given by (4.6), (4.7), (4.8), respectively. In the isotropic case, inserting $\mathbf{n}(\theta)$ and $\mathbf{F}(\delta; \lambda)$ into (5.3) (where we replace f by \tilde{W} or by W : since $\det \mathbf{F}(\delta; \lambda) \equiv 1$ this makes no difference), we obtain

$$\begin{aligned} G_{\delta\delta}(\lambda) &= \mu a^{1/3}, \\ G_{\delta\theta}(\lambda) &= -\mu a^{1/3} \left(\frac{a-1}{a} \right) \frac{a^{1/6}}{\lambda}, \\ G_{\theta\theta}(\lambda) &= \mu a^{1/3} \left(\frac{a-1}{a} \right) \left(\frac{a^{1/3}}{\lambda^2} - \lambda^2 \right), \end{aligned} \quad (5.8)$$

Thus, by (5.7), we have

$$G(\lambda) = \mu a^{1/3} (1 - g(\lambda)) \quad (5.9)$$

where

$$g(\lambda) := \frac{a-1}{a} \frac{a^{1/3}}{a^{1/3} - \lambda^4}. \quad (5.10)$$

Since $g(\lambda) = 1$ for $\lambda = a^{-1/6}$, and $g(\lambda)$ is strictly increasing in the interval $[a^{-\frac{1}{6}}, a^{\frac{1}{12}})$, we conclude that

$$G(a^{-\frac{1}{6}}) = 0, \quad \text{and} \quad G(\lambda) < 0, \quad \text{for every } \lambda \in (a^{-\frac{1}{6}}, a^{\frac{1}{12}}). \quad (5.11)$$

Considering energy \tilde{W}_β we obtain

$$\begin{aligned} G_{\delta\delta}^\beta(\lambda) &= \mu a^{1/3} + \frac{\beta\mu}{a^{2/3}}, \\ G_{\delta\theta}^\beta(\lambda) &= -\mu a^{1/3} \left(\frac{a-1}{a} \right) \frac{a^{1/6}}{\lambda}, \\ G_{\theta\theta}^\beta(\lambda) &= \mu a^{1/3} \left(\frac{a-1}{a} \right) \left(\frac{a^{1/3}}{\lambda^2} - \lambda^2 \right), \end{aligned} \quad (5.12)$$

so that, by (5.7), we have

$$G^\beta(\lambda) = \mu a^{1/3} \left(1 - g(\lambda) + \frac{\beta}{a} \right). \quad (5.13)$$

Since $g(\lambda)$ is strictly increasing in the interval $[a^{-\frac{1}{6}}, a^{\frac{1}{12}})$ starting from the value $g(a^{-\frac{1}{6}}) = 1$, and it diverges as $\lambda \rightarrow a^{\frac{1}{12}}$, we conclude that there exists $\lambda_c^\beta \in (a^{-\frac{1}{6}}, a^{\frac{1}{12}})$ such that

$$G^\beta(\lambda) > 0, \quad \text{for } \lambda \in [a^{-\frac{1}{6}}, \lambda_c^\beta), \quad \text{and} \quad G^\beta(\lambda) < 0, \quad \text{for } \lambda \in (\lambda_c^\beta, a^{\frac{1}{12}}). \quad (5.14)$$

The critical stretch λ_c^β is obtained by solving $g(\lambda_c^\beta) = 1 + \beta/a$ yielding

$$\lambda_c^\beta = a^{\frac{1}{12}} \left(\frac{\beta + 1}{\beta + a} \right)^{\frac{1}{4}}. \quad (5.15)$$

As β increases from 0 to ∞ , λ_c^β increases from $a^{-1/6}$ to $a^{1/12}$. Repeating the same procedure for energy \tilde{W}_α given by (4.8) we obtain

$$G^\alpha(\lambda) = \mu a^{\frac{1}{3}} \left[1 - \frac{a-1}{a} \frac{a^{1/3} + \alpha \frac{a^{2/3}}{a-1} \lambda^2 + \alpha \frac{a^{1/3}}{a-1} \lambda^6}{a^{1/3} + \alpha \frac{a^{2/3}}{a-1} \lambda^2 - \lambda^4} \right]. \quad (5.16)$$

Again, it turns out that there exists $\lambda_c^\alpha \geq a^{-1/6}$ such that

$$G^\alpha(\lambda) > 0, \quad \text{for } \lambda < \lambda_c^\alpha, \quad \text{and} \quad G^\alpha(\lambda) < 0, \quad \text{for } \lambda > \lambda_c^\alpha. \quad (5.17)$$

The critical stretch λ_c^α is an increasing function of α and, as α increases from 0 to ∞ , λ_c^α increases from $a^{-1/6}$ to the value

$$\lambda_c^\alpha = \frac{1}{(a-1)^{\frac{1}{4}}} a^{\frac{1}{12}}, \quad \alpha = \infty. \quad (5.18)$$

The corresponding values of $G^\alpha(\lambda)$ are

$$G^\alpha(\lambda) = \mu a^{\frac{1}{3}} \left[1 - \frac{a-1}{a} \frac{a^{\frac{1}{3}}}{a^{\frac{1}{3}} - \lambda^4} \right], \quad \alpha = 0, \quad (5.19)$$

$$G^\alpha(\lambda) = \mu a^{\frac{1}{3}} \left[1 - \frac{a-1}{a} \frac{a^{\frac{1}{3}} + \lambda^4}{a^{\frac{1}{3}}} \right], \quad \alpha = +\infty. \quad (5.20)$$

If the anisotropy parameter a is sufficiently large, say, $a \geq 2$, then the value of λ_c^α for $\alpha = +\infty$ is not larger than $a^{\frac{1}{12}}$ and we have that $\lambda_c^\alpha \leq a^{\frac{1}{12}}$ for all $\alpha \geq 0$. Using the values $\alpha = 1$ and $a = 2$ we obtain

$$0.89 = a^{-\frac{1}{6}} < \lambda_c^\alpha = 0.9637 < a^{\frac{1}{12}} = 1.06, \quad \alpha = 1, \quad a = 2. \quad (5.21)$$

The shear moduli calculated above, which become negative for certain values of the stretching parameter λ , show that the isotropic energy W leads

to material instabilities: uniformly stretched states become unstable to superposed shears. In other words, the stripe-domain instabilities discussed in Section 2, and analyzed in detail in the literature on nematic elastomers (see, [29], the discussion in [30, Chapter 7] and the analysis in [14],[6], and [8]) represent a form of elastic, reversible, shear band instability.

Indeed, consider the case of a sample which is uniformly stretched, starting from the natural state corresponding to $\mathbf{N} = \mathbf{N}_a = \mathbf{e}_3 \otimes \mathbf{e}_3$, according to the deformation gradient

$$\mathbf{F}(0; \lambda) = \begin{bmatrix} a^{-\frac{1}{6}} & 0 & 0 \\ 0 & \lambda & 0 \\ 0 & 0 & a^{\frac{1}{6}}/\lambda \end{bmatrix}, \quad (5.22)$$

with $\lambda \geq a^{-1/6}$. The occurrence of shear-like instabilities can be detected from the stability condition (5.11), which shows that the state $(\mathbf{F}(0; \lambda), \mathbf{N}_a)$ is unstable for every $\lambda > a^{-\frac{1}{6}}$.

The anisotropic corrections impart to the material a positive shear modulus up to a critical stretch λ_c . At this critical stretch, the modulus for shearing in planes containing \mathbf{n}_r vanishes, and a stripe domain instability with alternating shears becomes the mode of response of lowest energy to further stretching. This scenario is consistent both with the theoretical analyses in [21] and [30], and with the experimental results in [27]: with the anisotropic corrections, the soft mode of response of the ideally soft limit is latent in the initial configuration, and it is activated at a sufficiently large imposed stretch.

It is interesting to observe that this very transparent picture emerges naturally from a simple analysis of two fully nonlinear anisotropic energies, and from the geometric structure of the associated energy landscape. Figures 4 and 5 provide a concrete representation of such energy landscapes through the level curves of the functions

$$f(\delta, \lambda) := \min_{\theta} \tilde{W}(\mathbf{F}(\delta; \lambda), \mathbf{N}(\theta)) - \frac{3}{2}\mu \quad (5.23)$$

and

$$f_{\beta}(\delta, \lambda) := \min_{\theta} \tilde{W}_{\beta}(\mathbf{F}(\delta; \lambda), \mathbf{N}(\theta)) - \frac{3}{2}\mu(1 + \beta) \quad (5.24)$$

obtained by evaluating energies (4.6) and (4.7) on states described by (5.1) and (5.2), and optimizing with respect to θ . The functions $G(\lambda)$ and $G_{\beta}(\lambda)$ used in this Section (and also in Section 8 for the interpretation of the key experimental evidence available on nematic elastomers) give the curvature of the graphs of (5.23) and (5.24) along the line $\delta = 0$, and they enable

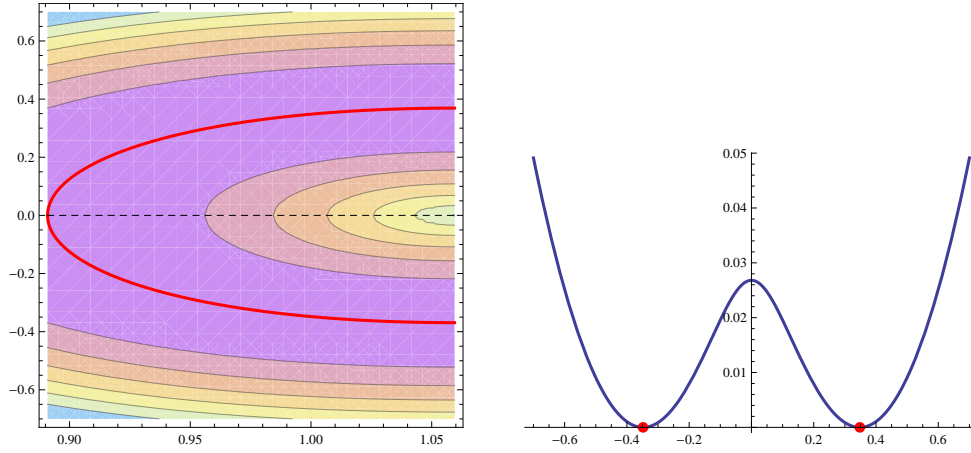


Figure 4: Energy landscape for the (ideally soft) isotropic energy (5.23) with $a = 2$ and $\mu = 1$. Equally spaced level curves in a plane (λ, δ) (left); graph of the section at $\lambda = 1$ (right). Energy minimizing states are shown by the thick red curve (left) and the red dots (right).

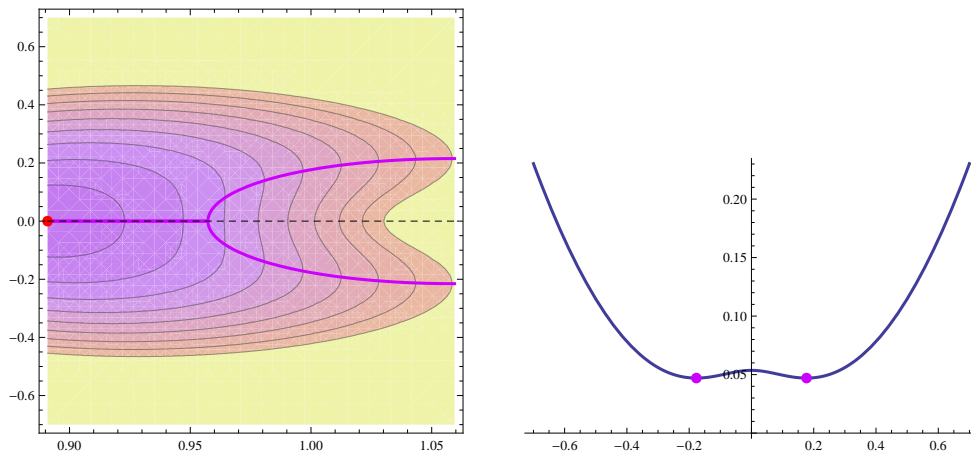


Figure 5: Energy landscape for the anisotropic energy (5.24) with $a = 2$, $\mu = 1$, and $\beta = 1$. Equally spaced level curves in a plane (λ, δ) (left); graph of the section at $\lambda = 1$ (right). The unique energy minimizing state is shown by the red dot; local minimizers at constant λ are shown by the thick purple curve (left) and the purple dots (right).

us to identify the material instabilities associated with the non-convexity of energies (4.6) and (4.7).

The results discussed above are fully consistent with [32, 2], where the effects of compositional fluctuations or of the aligning fields arising with the cross-linking process are discussed. We notice in addition that the analysis of the stability of equilibria with $\theta = \pi/2$ in a neighborhood of $\lambda = a^{1/3}$ (the stretch defining the upper limit of the plateau in the ideally soft case, see next section) is completely analogous to the one we have explicitly performed here, leading to similar instabilities and to another critical stretch defined by a vanishing shear modulus. Moreover, while our quantitative analysis is based on some simple concrete energy expressions, the qualitative picture that emerges is much more general, and it will be shared by a much larger class of energies.

The energy landscapes in Figures 4 and 5 enable us also to unfold the bifurcation occurring at fixed imposed stretch λ , and to anticipate the ensuing post-critical behavior. Indeed, the intersection of a vertical line through $(\lambda, 0)$ with the pitchforks in the graphs identify two co-operative shears $\pm\delta(\lambda)$, which are kinematically compatible and average to zero if occurring in bands of equal width. With these two opposite shears, we can uniquely associate two symmetric orientations $\pm\theta(\lambda)$ of the nematic director, where $\theta(\lambda)$ is the minimizer in (5.23) or (5.23) corresponding to $\mathbf{F}(\delta(\lambda); \lambda)$. These two orientations of the nematic director give rise to the optical contrast observed in the stripe-domain instability. A more complete analysis of this post-bifurcation mode of response, based on co-operative elastic shear banding will be the object of the next Section.

6 Effective energy: coarse-graining and quasi-convexification

We return now to the basic expression (4.1) for the elastic energy density in the incompressible case. For fixed \mathbf{F} , we minimize with respect to \mathbf{n} to obtain the effective energy

$$W_{\text{eff}}(\mathbf{F}) = \min_{|\mathbf{n}|=1} \left(W(\mathbf{F}, \mathbf{N}) - \frac{3}{2}\mu \right). \quad (6.1)$$

More explicitly,

$$W_{\text{eff}}(\mathbf{F}) = \begin{cases} \frac{\mu}{2} a^{1/3} (\lambda_1^2(\mathbf{F}) + \lambda_2^2(\mathbf{F}) + a^{-1} \lambda_3^2(\mathbf{F}) - 3a^{-1/3}) & \text{if } \det \mathbf{F} = 1 \\ +\infty & \text{else} \end{cases} \quad (6.2)$$

where the $\lambda_i(\mathbf{F})$ are the ordered principal stretches (in particular, $\lambda_3 = \lambda_{max}$). We remark that, if one evaluates (6.2) on deformation gradients $\mathbf{F}(\delta; \lambda)$ of the form (5.2), one obtains precisely the graph of Figure 4. In other words, $W_{\text{eff}}(\mathbf{F}(\delta; \lambda)) = f(\delta, \lambda)$, where f is given by (5.23). Moreover, the \mathbf{n} that achieves the minimum in (6.1) is the eigenvector \mathbf{n}_{opt} associated with the largest eigenvalue of $\mathbf{F}\mathbf{F}^T$:

$$\mathbf{F}\mathbf{F}^T \mathbf{n}_{opt} = \lambda_{max}^2(\mathbf{F}) \mathbf{n}_{opt} \quad (6.3)$$

The shear banding instabilities described in the previous section are related to the non-convexity of the energy landscape, as Figure 4 illustrates rather clearly. A useful notion of material stability is the quasiconvexity of the governing energy density. This is an infinite-dimensional analogue of the patch-test for finite elements. It means that an affine state of deformation \mathbf{F} gives the minimal energy state in a sample if one prescribes at its boundary affine displacement boundary conditions compatible with \mathbf{F} . As discussed in the previous section, (6.2) cannot be quasiconvex because it can be lowered by development of shear bands.

The quasiconvex envelope of W_{eff}

$$W_{\text{eff}}^{\text{qc}}(\mathbf{F}) = \inf_{\mathbf{y}} \left\{ \frac{1}{|\Omega|} \int_{\Omega} W_{\text{eff}}(\nabla \mathbf{y}(x)) dx : \mathbf{y}(x) = \mathbf{F}x \text{ on } \partial\Omega, \det \nabla \mathbf{y}(x) = 1 \right\}, \quad (6.4)$$

coarse-grains the energetics of the system: it gives the minimum energy needed to produce the macroscopic deformation \mathbf{F} , optimized over all possible admissible microstructures $\mathbf{y}(x)$. The infimum in (6.4) is taken over all functions \mathbf{y} that are Lipschitz-continuous. Note also that the domain Ω , whose volume we denote by $|\Omega|$, plays here the role of a representative volume element: it can be verified that $W_{\text{eff}}^{\text{qc}}$ does not depend on Ω . The use of $W_{\text{eff}}^{\text{qc}}$ in numerical computations allows one to resolve only the macroscopic length scale, with the (possibly infinitesimal) microscopic scale already accounted for in $W_{\text{eff}}^{\text{qc}}$. Clearly, this approach gives only average information on the fine phase mixtures and focuses on the macroscopic response of the system.

An explicit formula for the quasi-convex envelope of (6.2) has been derived in [14]. For volume-preserving deformation gradients it reads

$$W_{\text{eff}}^{\text{qc}}(\mathbf{F}) = \begin{cases} 0 & \text{(phase L) if } \lambda_1 \geq a^{-1/6} \\ W_{\text{eff}}(\mathbf{F}) & \text{(phase S) if } a^{-1/2} \lambda_3^2 \lambda_1 > 1 \\ \frac{\mu}{2} a^{1/3} (\lambda_1^2 + 2a^{-1/2} \lambda_1^{-1} - 3a^{-1/3}) & \text{(phase I) else} \end{cases} \quad (6.5)$$

while $W_{\text{eff}}^{\text{qc}}(\mathbf{F}) = +\infty$ if $\det \mathbf{F} \neq 1$. Here the labels L, S, and I refer to the fact that the resulting material response is liquid-like, solid-like, or of an intermediate type, see the discussion below.

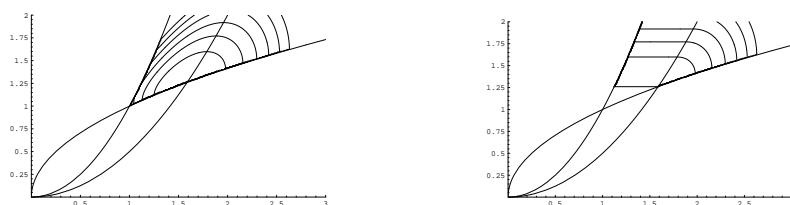


Figure 6: Level curves of the energy W_{eff} given by (6.2) (left) and of its quasiconvex envelope $W_{\text{eff}}^{\text{qc}}$ given by (6.5) (right).

The formula above gives a very precise picture of the macroscopic mechanical response resulting from our model, and of its microscopic origin. There are three regimes in (6.5), arising from the collective behavior of energetically optimal fine phase mixtures. They represent three different modes of macroscopic mechanical response, corresponding to three different patterns of microscopic decomposition of the macroscopic deformation gradient \mathbf{F} . Phase L describes a liquid-like response (at least within the ideally soft approximation underlying expression (6.2) for the microscopic energy density; a more realistic semi-soft case is discussed in [7]). All gradients falling in this region of the phase diagram, which is the zero level set of W_{qc} , can be sustained at zero internal stress. To resolve microscopically the whole of phase L (in particular, to resolve the deformation gradient $\mathbf{F} = \text{Id}$) it is necessary to allow for relatively complex microstructures (layers-within-layers). Phase S describes a solid-like response in which fine phase mixtures are ruled out. As a consequence, in this regime the coarse-grained macroscopic energy W_{qc} reproduces the microscopic energy W_{eff} with no changes. Finally, gradients in the intermediate phase I can transmit stresses (unlike phase L) through microstructure formation (unlike phase S). The microscopic patterns required to resolve phase I have a relatively simple geometry (laminates, or simple-layers) Patterns of this kind have been frequently observed experimentally after being first reported in [24]. The first attempt to explain them through elastic energy minimization is in [29].

The expression (6.5) for the energy density has been used in [6] for the numerical simulation of stretching experiments of sheets of nematic elastomer held between two rigid clamps. The simulations are designed to reproduce the classical experimental setting of Kundler and Finkelmann [24], where stripe-domain patterns were first observed.

The specimen is a thin sheet of nematic elastomer. We choose a reference frame with axis x_1 parallel to the thickness direction. Moreover, we assume that the specimen is prepared with the director uniformly aligned along x_3 , and is then stretched along x_2 . By reorienting the director from the x_3 to the x_2 direction, the material can accommodate the imposed stretches without storing elastic energy. As it is well known, see e.g. [30], a uniform rotation of the director would induce large shears, which are incompatible with the presence of the clamps. Director reorientation occurs instead with the development of spatial modulations shaped as bands parallel to the x_2 axis. This is the origin of the striped texture observed in the experiments.

The numerical simulations allow us to analyze the stretching experiments in more detail. If the clamps do not allow lateral contraction, the reorientation of the director towards the direction of the imposed stretch is severely hindered. This constraint is stronger near the clamps, and it decays away

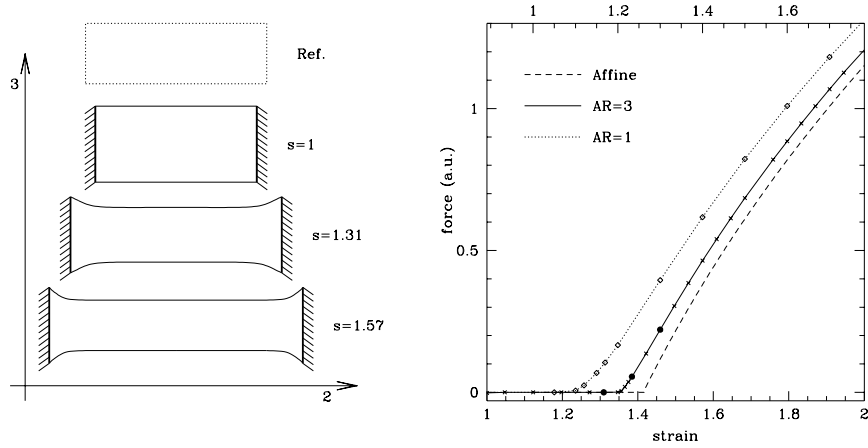


Figure 7: Numerical simulation of stretching experiments on thin sheets of nematic elastomers: geometry (left) and force–stretch diagrams for several aspect ratios AR (right). The panel on the left shows four configurations, namely, reference, initial, and the two at stretches $s=1.31$ and $s=1.57$ for the geometry with $AR=3$. On the corresponding force–stretch curve on the right panel, full dots mark the representative points of configurations shown in Figure 8 (adapted from [6]).

from them producing two interesting effects. On the one hand, the induced microstructures are spatially inhomogeneous, with director reorientation occurring more rapidly in the regions far away from the clamps. On the other hand, the stress–strain response shows a marked dependence on the geometry of the sample, with the influence of the clamps becoming less pronounced as the aspect ratio length/width increases. These effects are documented in Figure 7 and Figure 8, which show good qualitative agreement with both the experimental results from the Cavendish Laboratories [30], and with the X-ray scattering measurements in [33].

The stripe domain patterns appearing in Figure 8 are all simple laminates, either in phase L or in phase I. Focussing on the point at the center of the sample (the bottom left corner in the plots of the deformed shape), the material is in phase L as long as no force is transmitted at the clamps. The

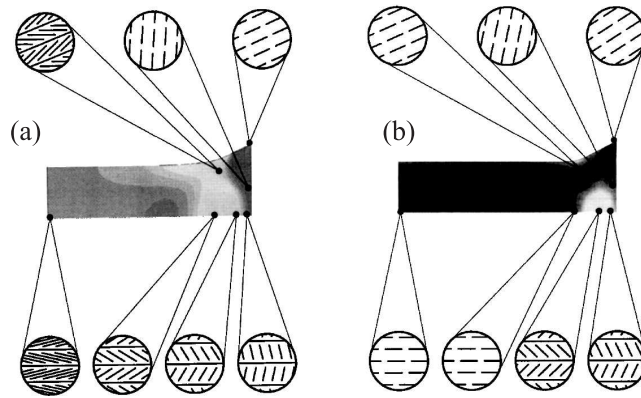


Figure 8: Numerical simulation of stretching experiments on thin sheets of nematic elastomers, based on the coarse-grained energy $W_{\text{eff}}^{\text{qc}}$, at stretches $s=1.31$ (a), and $s=1.38$ (b). Only one-quarter of the sample is shown since the rest of the solution can be obtained by symmetry. The circular insets display energetically optimal microstructures at some selected locations within the sample. The sticks give the local orientation of the principal direction of maximal stretch, i.e., the orientation of the nematic director (adapted from [6]).

computed deformation gradient is

$$\mathbf{F}_\lambda = \begin{pmatrix} a^{-1/6} & 0 & 0 \\ 0 & \lambda & 0 \\ 0 & 0 & a^{1/6}/\lambda \end{pmatrix} \quad (6.6)$$

with λ varying from $a^{-1/6}$ to $a^{1/3}$. This is resolved by a simple laminate in which the deformation gradient oscillates between the values

$$\mathbf{F}_\lambda^\pm = \begin{pmatrix} a^{-1/6} & 0 & 0 \\ 0 & \lambda & \pm\delta \\ 0 & 0 & a^{1/6}/\lambda \end{pmatrix} \quad (6.7)$$

in stripes perpendicular to x_3 . The value of $\delta = \delta(\lambda)$ is obtained from $\delta^2 = (a^{2/3} - \lambda^2)(1 - a^{-1/3}\lambda^{-2})$, which ensures that \mathbf{F}_λ^\pm has the characteristic principal stretches giving $W_{\text{eff}}(\mathbf{F}_\lambda^\pm) = 0$. Notice that the kinematic compatibility condition $\mathbf{F}_\lambda^+ - \mathbf{F}_\lambda^- = \mathbf{a} \otimes \hat{\mathbf{n}}$, where $\hat{\mathbf{n}}$ is the reference normal to the stripes and \mathbf{a} is a shear vector, is satisfied with $\mathbf{a} = 2\delta(\lambda)\mathbf{e}_2$ and $\hat{\mathbf{n}} = \mathbf{e}_3$. This guarantees the existence of a continuous map \mathbf{y} such that either $\nabla\mathbf{y}(\mathbf{x}) = \mathbf{F}_\lambda^+$, or $\nabla\mathbf{y}(\mathbf{x}) = \mathbf{F}_\lambda^-$, with $\nabla\mathbf{y}$ constant in layers with normal \mathbf{e}_3 . The deformation patterns given by (6.7) characterize the systems of shear bands resolving the post-critical behavior of the material following the shear band instability described in the previous sections. Associated with that, one finds a modulated pattern $\mathbf{n}_{\text{opt}}(\mathbf{F}_\lambda^\pm)$ for the nematic director, where \mathbf{n}_{opt} is given by (6.3).

Force starts being transmitted through the sample when the deformation gradient in the central point moves to the region I of the phase diagram. The computed deformation gradient is now of the form

$$\mathbf{F}_1(\lambda_1) = \begin{pmatrix} \lambda_1 & 0 & 0 \\ 0 & 1/\lambda_1\lambda_3 & 0 \\ 0 & 0 & \lambda_3 \end{pmatrix} \quad (6.8)$$

where $\lambda_3 > a^{1/3}$ forces $\lambda_1 < a^{-1/6}$. This is resolved by simple laminates similar to the ones above. The deformation gradient oscillates between the values

$$\mathbf{F}_1^\pm(\lambda_1) = \begin{pmatrix} \lambda_1 & 0 & 0 \\ 0 & 1/\lambda_1\lambda_3 & \pm\delta \\ 0 & 0 & \lambda_3 \end{pmatrix} \quad (6.9)$$

in stripes perpendicular to x_3 , and $\delta = \delta(\lambda_1)$ is computed by requiring that the principal stretches be those giving the minimal energy at given λ_1 , namely, $(\lambda_1, a^{-1/4}\lambda_1^{-1/2}, a^{1/4}\lambda_1^{-1/2})$, see [6]. The associated nematic texture is again obtained from $\mathbf{n}_{\text{opt}}(\mathbf{F}_1^\pm(\lambda_1))$, with \mathbf{n}_{opt} given by (6.3).

A relaxation result providing the small strain analog of (6.5) has been obtained in [4]. Anisotropic corrections leading to more realistic force-stretch curves, in which the soft plateau occurs at small but finite levels of force are discussed in [7].

7 Dynamics under an applied electric field

In order to move the first steps towards modeling the dynamic response of nematic elastomers to applied electric fields, we follow [12] and use a simpler, geometrically linear theory. This small-strain approximation has been used to study the equilibrium response to applied electric fields in [5]. The same approach has been used quite successfully in [20] to reproduce the experimentally measured dynamic response of nematic gels to applied electric fields.

We consider a sample of a nematic gel occupying a region \mathcal{B} inside a cell Ω . The part $\Omega \setminus \mathcal{B}$ of the cell is occupied by an isotropic dielectric (typically, silicon oil). We denote by \mathbf{u} and \mathbf{n} the displacement and the nematic director in \mathcal{B} , and by φ the electric potential in Ω . As usual, \mathbf{n} is parametrized through a rotation field \mathbf{R} such that $\mathbf{n} = \mathbf{R}\mathbf{n}_r$, where \mathbf{n}_r is a (fixed) reference orientation.

The governing equations of our model are Gauss' law for an anisotropic dielectric, the standard balance of linear momentum for a viscoelastic solid, and an evolution equation modeling a viscous-like dynamics for the director rotation. They read as

$$\operatorname{div}(\mathbf{d}) = 0 \quad (7.1)$$

in Ω , and

$$\operatorname{div}(\mathbf{S}) = 0, \quad (7.2)$$

$$\begin{aligned} \eta_n(\dot{\mathbf{R}}\mathbf{R}^\top - \mathbf{W}_{\dot{\mathbf{u}}}) &= [\mathbf{S}, \mathbf{E}_0] + \frac{1}{2} \varepsilon_o \varepsilon_a [\nabla\varphi \otimes \nabla\varphi, \mathbf{n} \otimes \mathbf{n}] \\ &+ \operatorname{skw}(\operatorname{div}(k_F \nabla\mathbf{n}) \otimes \mathbf{n}) \end{aligned} \quad (7.3)$$

in \mathcal{B} . They are supplemented by suitable initial and boundary conditions, adapted to the specific experimental set-up one is trying to model. Here, in (7.1), the electric displacement \mathbf{d} is given by

$$\mathbf{d} = -\varepsilon_o \mathbb{D}\nabla\varphi, \quad (7.4)$$

with

$$\mathbb{D}\nabla\varphi = \begin{cases} \varepsilon_\perp \nabla\varphi + \varepsilon_a (\nabla\varphi \cdot \mathbf{n}) \mathbf{n} & \text{in } \mathcal{B}, \\ \varepsilon_c \nabla\varphi & \text{in } \Omega \setminus \mathcal{B}, \end{cases} \quad (7.5)$$

where $\varepsilon_o > 0$ is the free space permittivity, ε_{\parallel} and ε_{\perp} are the relative permittivities of the gel in the directions parallel and perpendicular to \mathbf{n} , $\varepsilon_a = \varepsilon_{\parallel} - \varepsilon_{\perp}$ is the dielectric anisotropy, and ε_c is the relative permittivity of the isotropic dielectric occupying the region $\Omega \setminus \mathcal{B}$.

Moreover, in (7.2) and (7.3), $\mathbf{E}_0 = \mathbf{E}_0(\mathbf{n})$ is the spontaneous strain associated with the isotropic-to-nematic transformation

$$\mathbf{E}_0(\mathbf{n}) = \frac{3}{2}\gamma \left(\mathbf{n} \otimes \mathbf{n} - \frac{1}{3} \mathbf{I} \right), \quad (7.6)$$

while the stress \mathbf{S} is given by

$$\mathbf{S} = \mathbb{C} (\mathbf{E}_{\mathbf{u}} - \mathbf{E}_0) + \eta_g \mathbf{E}_{\dot{\mathbf{u}}}, \quad (7.7)$$

where

$$\mathbf{E}_{\mathbf{u}} = \frac{1}{2} \left(\nabla \mathbf{u} + (\nabla \mathbf{u})^{\top} \right), \quad (7.8)$$

$$\mathbf{E}_{\dot{\mathbf{u}}} = \frac{1}{2} \left(\nabla \dot{\mathbf{u}} + (\nabla \dot{\mathbf{u}})^{\top} \right), \quad (7.9)$$

\mathbb{C} is the (positive definite) tensor of elastic moduli, and $\eta_g > 0$ is the viscosity of the gel. In principle, one would like to assume for $\mathbb{C} = \mathbb{C}(\mathbf{n})$ the symmetry of a transversely isotropic solid with distinguished axis \mathbf{n} , so that the Cartesian components of \mathbb{C} are all described in terms of five independent scalars. Since a detailed experimental characterization of these parameters is not available, whenever quantitative information on them is needed for our analysis, we make the simplifying assumptions $C_{33} = C_{11}$, $C_{12} = C_{13}$, and $C_{66} = C_{44} = (C_{11} - C_{12})/2$ (see, e.g., [23, Ch. 3]; here we are using Voigt's notation for the components of \mathbb{C} , and assuming that \mathbf{n} is directed along the third coordinate axis). In this case, \mathbb{C} becomes isotropic, denoted by \mathbb{C}_{iso} , and the values of the Young modulus Y and the Poisson ratio ν suffice to fully characterize \mathbb{C}_{iso} .

Finally, in (7.3), $\eta_n > 0$ denotes a parameter describing the rotational viscosity of the director, $\dot{\mathbf{R}}$ denotes the time rate of \mathbf{R} , $\mathbf{W}\dot{\mathbf{u}}$ is the skew-symmetric part of the velocity gradient $\nabla \dot{\mathbf{u}}$, k_F is the Frank constant (giving the strength of curvature elasticity in the one-constant approximation adopted here), $\text{skw}(\mathbf{A}) = (\mathbf{A} - \mathbf{A}^{\top})/2$ denotes the skew-symmetric part of the matrix \mathbf{A} , and $[\mathbf{A}, \mathbf{B}] = \mathbf{A}\mathbf{B} - \mathbf{B}\mathbf{A}$ is the commutator of the matrices \mathbf{A} and \mathbf{B} .

The model above is derived as follows. We introduce the total energy functional

$$\begin{aligned} \mathcal{E} &= \frac{1}{2} \int_{\mathcal{B}} \left(k_F |\nabla \mathbf{n}|^2 + \mathbb{C} (\mathbf{E}_{\mathbf{u}} - \mathbf{E}_0) \cdot (\mathbf{E}_{\mathbf{u}} - \mathbf{E}_0) \right) \\ &\quad - \frac{1}{2} \int_{\Omega} \left(\varepsilon_o (\mathbb{D} \nabla \varphi) \cdot \nabla \varphi \right) - \int_{\partial_s \mathcal{B}} (\mathbf{s}_{ext} \cdot \mathbf{u}), \end{aligned} \quad (7.10)$$

where the first summand contains Frank's curvature energy and the elastic energy the second one is the total electric energy including the energy needed to maintain the constant voltage difference V across the cell, see [10, eq. (3.67)] and [28, eq. (2.86)], and the third one is the potential energy of the loading device exerting an external force per unit area, denoted by \mathbf{s}_{ext} , on the loaded part $\partial_s \mathcal{B}$ of the boundary of \mathcal{B} . When $\mathbb{C} = \mathbb{C}_{iso}$ the elastic energy term in (7.10) reduces to $\tilde{\Phi}$ given by (4.15).

Equations (7.1) and (7.2) are standard. The first one arises by assuming instantaneous relaxation to equilibrium of the electric potential and a viscoelastic dynamics for the elastic displacement

$$0 = \frac{\delta \mathcal{E}}{\delta \varphi}, \quad (7.11)$$

$$\frac{\delta \mathcal{D}}{\delta \dot{\mathbf{u}}} = -\frac{\delta \mathcal{E}}{\delta \mathbf{u}}, \quad (7.12)$$

where the operator δ is used to denote the variational derivatives of the energy functional \mathcal{E} with respect to φ and \mathbf{u} , and the variational derivative of the viscous dissipation \mathcal{D}

$$\mathcal{D} = \eta_n |\dot{\mathbf{R}}\mathbf{R}^\top - \mathbf{W}_{\dot{\mathbf{u}}}|^2 + \eta_g |\mathbf{E}_{\dot{\mathbf{u}}}|^2 \quad (7.13)$$

with respect to $\dot{\mathbf{u}}$. Straightforward manipulations show that (7.12) is equivalent to (7.2) supplemented by the constitutive assumptions (7.6)–(7.7). Similarly, (7.3) follows from

$$\frac{\delta \mathcal{D}}{\delta \dot{\mathbf{n}}} = -\frac{\delta \mathcal{E}}{\delta \mathbf{n}}, \quad (7.14)$$

(notice that $\dot{\mathbf{R}}\mathbf{R}^\top \mathbf{n} = \dot{\mathbf{n}} = \boldsymbol{\omega} \times \mathbf{n}$, where $\boldsymbol{\omega}$ is the director angular velocity) which states that the dynamics is such that the “viscous” dissipation rate accompanying the director evolution balances exactly the energy release rate driving the process.

The structure of equation (7.3) reveals in a rather transparent way the conditions such that a spatially uniform director field \mathbf{n} be in equilibrium. In particular, the condition $[\mathbf{S}, \mathbf{E}_0] = 0$ is satisfied if and only if the stress \mathbf{S} and the spontaneous distortion $\mathbf{E}_0(\mathbf{n})$ have the same principal directions (see [22, p. 12]).

The model described above has been used in [20] to understand experiments performed on a free-standing film in which an applied field perpendicular to the initial orientation of the nematic director is switched on suddenly, maintained on until the system reaches equilibrium, and then switched off. The comparison between the predicted relaxation times of \mathbf{n} and \mathbf{u} following switch on and switch off and the experimental measurements is in Figure

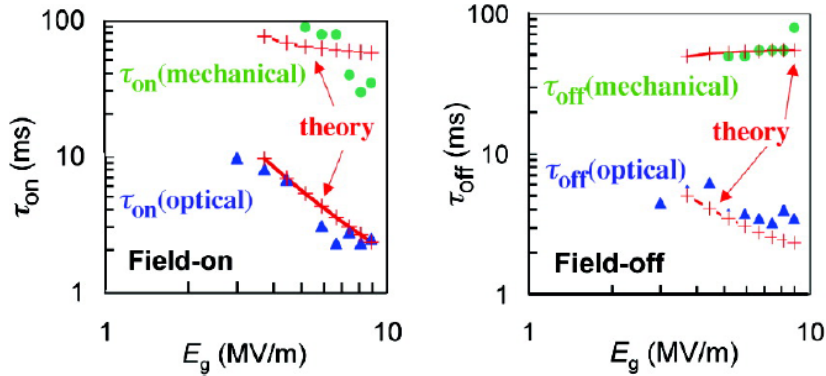


Figure 9: Characteristic relaxation times of \mathbf{n} (optical) and \mathbf{u} (mechanical) following to switch-on and switch-off of an electric field. Adapted from [20].

9. In order for this agreement to be possible, we need to use for the elastic energy the anisotropic expression $\tilde{\Phi}_\alpha$ (4.18) instead of either $\tilde{\Phi}(\mathbf{E}, \mathbf{N}) = \mathbb{C}_{iso}(\mathbf{E} - \mathbf{E}_0) \cdot (\mathbf{E} - \mathbf{E}_0)/2$ or $\tilde{\Phi}_\beta(\mathbf{E}, \mathbf{N}) = \tilde{\Phi}(\mathbf{E}, \mathbf{N}) + \mu_\beta |\mathbf{E}_d - \mathbf{E}_0(\mathbf{N}_a)|^2$. In spite of the anisotropic correction, this last expression does not provide a spring-back mechanism pushing the director back to the initial orientation \mathbf{n}_a when the electric field is switched off.

The dynamic model can be used also in the absence of applied electric fields to investigate rate effects in the force-stretch curves, and whether the response curves obtained in Section 6 by global energy minimization are also dynamically accessible in the limit of vanishingly small loading rates [16]. Interestingly, one may study in this way the dynamic pathways originating from an unstable state and leading to a new stable state. A stretching experiment giving a dynamic analogue of the one shown in Figure 7 is presented in Figure 10. A snapshot of dynamic simulations leading to formation of stripe domains is shown in Figure 11.

8 Comparison with key experimental results

We now compare the predictions of the various models discussed above with the experimental evidence coming from three benchmark experiments: purely mechanical stretching and shearing, and electric-field-induced rotation of the nematic director in a free-standing film.

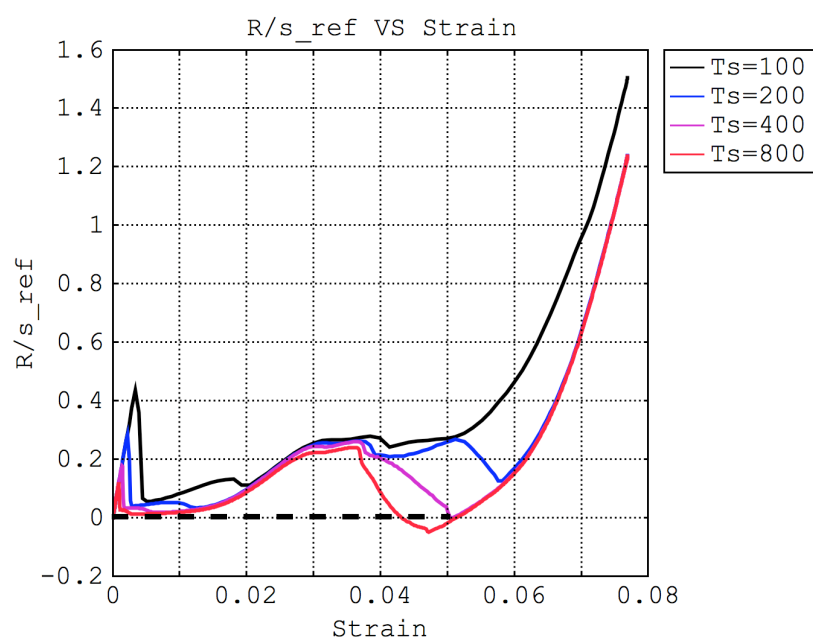


Figure 10: Dynamic force-strain response under purely mechanical stretching. The dashed line gives the response curve corresponding to global energy minimizers. Adapted from [16].

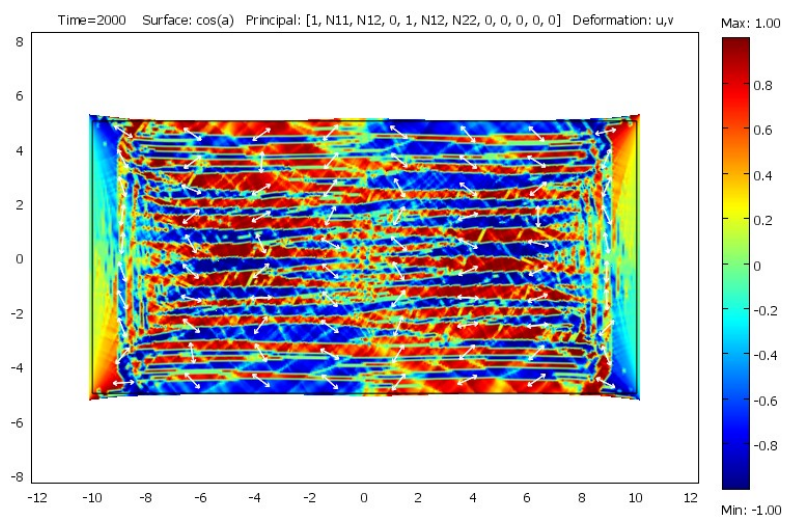


Figure 11: A snapshot from numerical simulations of dynamic stretching experiments at slow stretching rates, leading to formation of stripe domains. Adapted from [16].

8.1 Stretch

Consider a stretching experiment starting from the natural state corresponding to $\mathbf{N} = \mathbf{N}_r = \mathbf{e}_3 \otimes \mathbf{e}_3$ and described by the deformation gradient

$$\mathbf{F}(0; \lambda) = \begin{bmatrix} a^{-\frac{1}{6}} & 0 & 0 \\ 0 & \lambda & 0 \\ 0 & 0 & a^{\frac{1}{6}}/\lambda \end{bmatrix}, \quad (8.1)$$

with $\lambda \geq a^{-1/6}$. Here \mathbf{n}_r denotes an arbitrary reference orientation when dealing with the isotropic material; it will be chosen as $\mathbf{n}_r = \mathbf{n}_a$ when dealing with one of the anisotropic ones. The deformation described by (8.1) is a plane-strain extension or, in Treloar's terminology, a pure shear. As long as the state $(\mathbf{F}(0; \lambda), \mathbf{N} = \mathbf{N}_r)$ is a stable equilibrium, the stress response can be obtained from $W(\mathbf{F}(0; \lambda), \mathbf{N}_r)$ by differentiating with respect to λ . This leads to

$$\sigma(\lambda) = \mu \left(a^{\frac{1}{3}} \lambda - \frac{1}{a^{\frac{1}{3}} \lambda^3} \right), \quad (8.2)$$

where σ denotes the normal stress difference $S_{22} - S_{33}$ measured in terms of nominal (or first Piola-Kirchhoff) stresses.

As already discussed in the previous sections, the isotropic energy W leads to a stripe-domain instability: already at $\lambda = a^{-1/6}$, the homogeneous state $(\mathbf{F}(0; \lambda), \mathbf{N} = \mathbf{N}_r)$ loses stability in favor of nonhomogeneous patterns with alternating shears having the same average deformation as (8.1) but lower energies than the uniformly deformed state (8.1). These alternating shears play a crucial role in the calculation of the coarse-grained energy (the quasiconvex envelope) performed in Section 6. The analogy between this mode of response and mechanical twinning in materials exhibiting martensitic transformations has been first pointed out in [11]. Formula (8.2) does not apply and, thanks to the development of alternating shear bands of the form (6.7), the system can accommodate any stretch $\lambda \in [a^{-\frac{1}{6}}, a^{\frac{1}{3}}]$ at zero stress $\sigma(\lambda) \equiv 0$, thus exhibiting an ideally soft response.

Applying a similar argument to energy W_β we obtain instead

$$\sigma^\beta(\lambda) = \mu(1 + \beta) \left(a^{\frac{1}{3}} \lambda - \frac{1}{a^{\frac{1}{3}} \lambda^3} \right), \quad \lambda \in [a^{-\frac{1}{6}}, \lambda_c^\beta]. \quad (8.3)$$

This implies that the material will show a hard response up to the critical stretch λ_c^β . Then a softer mode of response, accompanied by the emergence of non-homogenous deformation patterns relying on alternating shears of the form $\mathbf{F}(\pm\delta; \lambda)$ given by (5.2), becomes energetically advantageous and dynamically accessible. The value λ_c^β is clearly an upper bound for the onset

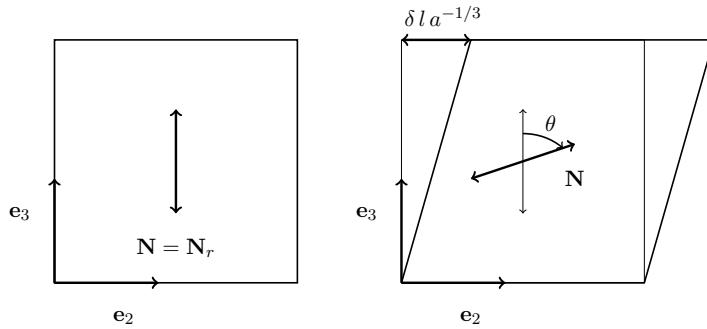


Figure 12: Shear experiment corresponding to (8.5) on a sample of initial size $h \times l \times l$.

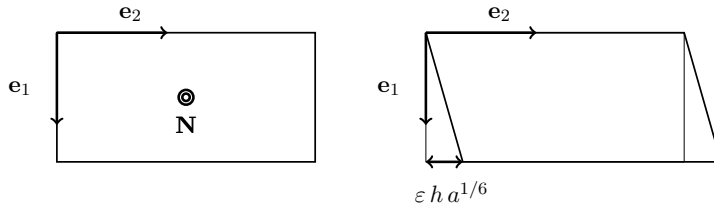


Figure 13: Shear experiment corresponding to (8.6) on a sample of initial size $h \times l \times l$.

of the instability because, in a real system, imperfections may trigger the instability well before λ_c^β is reached. Applying the same argument to \tilde{W}_α we obtain exactly the same scenario of a hard response only up to a threshold given by

$$\sigma^\alpha(\lambda) = \mu \left(a^{\frac{1}{3}} \lambda - \frac{1}{a^{\frac{1}{3}} \lambda^3} \right), \quad \lambda \in [a^{-\frac{1}{6}}, \lambda_c^\alpha]. \quad (8.4)$$

Estimates of the critical stretches λ_c^β , λ_c^α for meaningful values of the material parameters are given in (5.15) and (5.21). For stretches exceeding the critical value for the stability of a homogeneously stretched state, numerical simulations are needed in order to resolve the complex, non-homogeneous response.

8.2 Shear

We move now to simple shear experiments. Starting from the natural state corresponding to $\mathbf{N} = \mathbf{N}_r = \mathbf{e}_3 \otimes \mathbf{e}_3$, we consider simple shears of magnitude

proportional to δ in a plane containing \mathbf{n}_r

$$\mathbf{F}(\delta; a^{-\frac{1}{6}}) = \begin{bmatrix} a^{-\frac{1}{6}} & 0 & 0 \\ 0 & a^{-\frac{1}{6}} & \delta \\ 0 & 0 & a^{\frac{1}{3}} \end{bmatrix}, \quad (8.5)$$

and simple shears of magnitude proportional to ε in a plane perpendicular to \mathbf{n}_r

$$\tilde{\mathbf{F}}(\varepsilon; a^{-\frac{1}{6}}) = \begin{bmatrix} a^{-\frac{1}{6}} & 0 & 0 \\ \varepsilon & a^{-\frac{1}{6}} & 0 \\ 0 & 0 & a^{\frac{1}{3}} \end{bmatrix}. \quad (8.6)$$

In this second case, it turns out that $\mathbf{N} = \mathbf{N}_r$ is always an equilibrium and we obtain energy expressions of the form

$$f(\varepsilon, 0; \lambda) = f(0, 0; \lambda) + \frac{1}{2} \tilde{G} \varepsilon^2, \quad (8.7)$$

where

$$\tilde{G} = \mu a^{\frac{1}{3}}, \quad (8.8)$$

$$\tilde{G}^\beta = \mu(1 + \beta) a^{\frac{1}{3}}, \quad (8.9)$$

$$\tilde{G}^\alpha = \mu a^{\frac{1}{3}}. \quad (8.10)$$

The moduli for shears in a plane containing \mathbf{n}_r (recall that $\mathbf{n}_r = \mathbf{n}_a$ in anisotropic cases) follow from (5.9), (5.13), (5.16), and are given by

$$G = G(a^{-\frac{1}{6}}) = 0, \quad (8.11)$$

$$G^\beta = G^\beta(a^{-\frac{1}{6}}) = \frac{\beta\mu}{a^{\frac{2}{3}}}, \quad (8.12)$$

$$G^\alpha = G^\alpha(a^{-\frac{1}{6}}) = \alpha\mu \frac{1}{a^{\frac{2}{3}}(1 + a^2 - 2a + a\alpha)}. \quad (8.13)$$

From (8.9) and (8.12) it follows that

$$G^\beta = \frac{1}{a} \left(\frac{\beta}{1 + \beta} \right) \tilde{G}^\beta \quad (8.14)$$

so that, as β increases from 0 to $+\infty$, G^β increases from 0 to $\frac{1}{a} \tilde{G}^\beta$. Using a typical value $a = 2$ for a , we obtain that G^β can be as large as half of \tilde{G}^β , provided that β is large enough. From (8.10) and (8.13) it follows that

$$G^\alpha = \frac{\alpha}{a + a^3 - 2a^2 + a^2\alpha} \tilde{G}^\alpha \quad (8.15)$$

so that, as α increases from 0 to $+\infty$, G^α increases from 0 to $\frac{1}{a^2}\tilde{G}^\alpha$. For $\alpha = 1$ and $a = 2$ we deduce from (8.15) that $G^\alpha = \frac{1}{6}\tilde{G}^\alpha$.

These results show that the relatively large moduli reported in [27] for shears in planes containing \mathbf{n}_a are not incompatible with the theoretical estimates, provided that the anisotropy parameters α and β have large enough values.

8.3 Electric field applied to a free-standing film

The experiments reported in [20] provide another important conceptual benchmark. By applying an electric field to a free-standing film of a swollen nematic elastomer, in such a way that the electric field drives the director away from its initial orientation $\mathbf{n}_r = \mathbf{n}_a$, one obtains a very clean set-up where many features of the mechanics of nematic elastomers can be addressed unambiguously. The experiments confirm the power of formula (2.1) in reading correctly the coupling between mechanical deformations and nematic order, as shown by the good match between birefringence and strain at steady state as functions of the applied voltage, see Figure 14. Moreover, the experiments show that a finite critical field needs to be overcome in order to trigger director rotation, and that the director springs back to the initial orientation when the electric field is removed. Both these phenomena are a direct manifestation of anisotropy. Interestingly, of the two proposed anisotropic formulas, only (4.18) seems capable of capturing spring-back while, with (4.17), the spring-back mechanism is suppressed.

8.4 Discussion

Our analysis shows that the three experimental findings:

- existence of a finite threshold before the emergence of a softer mode of response to stretching,
- absence of a vanishingly small shear modulus in simple shear experiments starting from the natural state corresponding to the director orientation at cross-linking,
- existence of a finite threshold in electric-field induced rotation of the director in free-standing nematic gels,

are all related manifestations of the anisotropy imprinted in the material by memory of the cross-linking state, where $\mathbf{N} = \mathbf{n}_a \otimes \mathbf{n}_a$. Simple anisotropic corrections to the basic trace formula (4.1), which represents their isotropic,

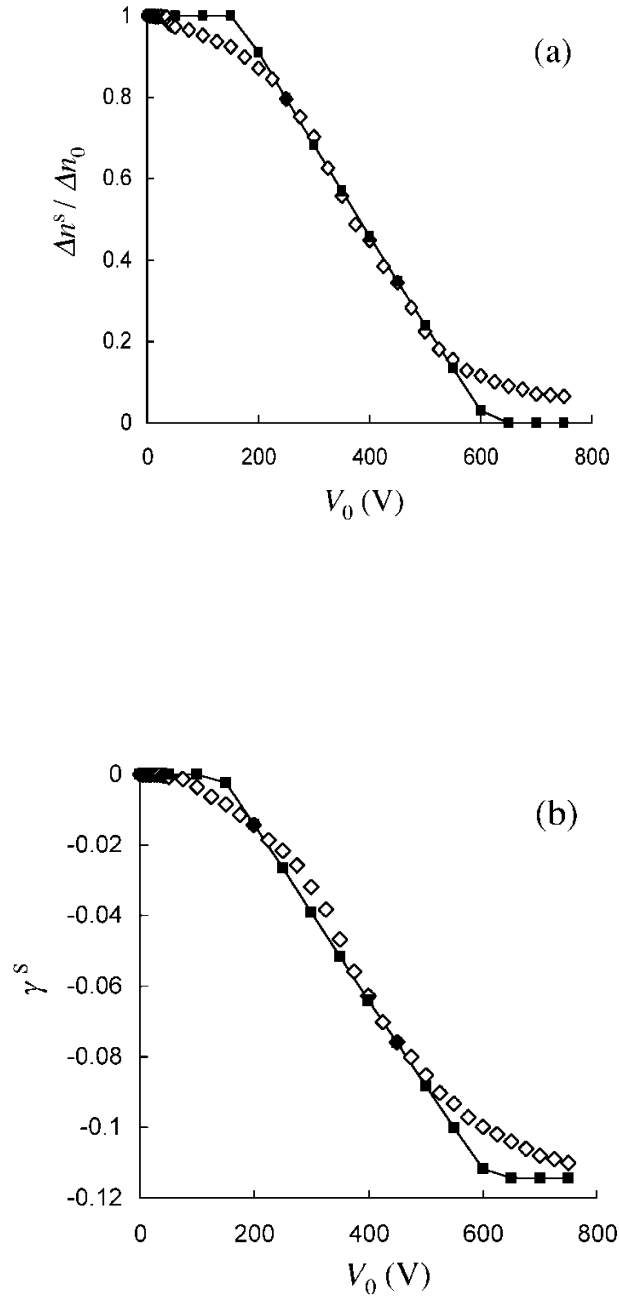


Figure 14: Birefringence (a) and strain (b) at steady state as functions of the applied voltage. Birefringence gives a direct measurement of \mathbf{n} and the correlation between the two curves is precisely the one implied by eq. (4.17). Adapted from [20].

or ideally soft limit, are able to reproduce (at least qualitatively) the available experimental evidence, and hence “explain” it.

We close by emphasizing again that the model anisotropic energies discussed here should not be considered as immediate tools for the faithful reproduction of the experimentally measured response of any specific sample. They are conceptual models. But, as a wise man once said, nothing is more practical than a good theory.

9 Appendix: alignment energies

In this appendix we discuss some examples of alignment energies, namely, energies whose minimization enforces alignment with a given vector \mathbf{n}_0 or a given tensor \mathbf{L} . In parametrizing the set of unit vectors it will be useful to remember that an arbitrary unit vector \mathbf{n} can be represented through the action of a rotation $\mathbf{R} \in \mathbb{R}ot$ acting on a fixed reference unit vector \mathbf{n} (for which one can take, e.g., one of the unit vectors of the canonical basis).

Let \mathbf{n}_0 , with $|\mathbf{n}_0| = 1$, be a given unit vector, let \mathbf{n} be an arbitrary unit vector, and consider the energy density

$$f(\mathbf{n}) = -\frac{k}{2}\mathbf{n} \cdot \mathbf{n}_0 = -\frac{k}{2}\cos^2\theta, \quad k > 0, \quad (9.1)$$

where θ is the smallest angle between $\pm\mathbf{n}$ and $\pm\mathbf{n}_0$. Since $\cos^2\theta \leq 1$, we have that $f \geq -k/2$ with equality achieved only by $\mathbf{n} = \pm\mathbf{n}_0$. An important example is provided by the electrostatic energy density of an anisotropic dielectric in the case of positive dielectric anisotropy $\varepsilon_a > 0$. Indeed, the electrostatic energy density reads

$$f_{ele}(\mathbf{n}) = -\frac{\varepsilon_o|\mathbf{E}|^2}{2}(\varepsilon_\perp + \varepsilon_a(\mathbf{n} \cdot \mathbf{n}_0)), \quad \mathbf{n}_0 = \frac{\mathbf{E}}{|\mathbf{E}|}, \quad (9.2)$$

where \mathbf{E} is the electric field while ε_o , ε_\perp , and ε_a are dielectric constants. For $\varepsilon_a > 0$, $f_{ele}(\mathbf{n})$ is minimized by $\mathbf{n} = \pm\mathbf{E}/|\mathbf{E}|$. This shows that energy (9.2) enforces a *quadrupolar* coupling between director \mathbf{n} and electric field \mathbf{E} .

We now move to energies encoding the alignment effect on the state of deformation \mathbf{F} due to a spontaneous or an externally imposed uniaxial tensor field \mathbf{L} . The typical example is

$$\mathbf{L} = \mathbf{R}\mathbf{L}_r\mathbf{R}^T, \quad \mathbf{L}_r = \mathbf{V}_r^2 = a^{2/3}\mathbf{N}_r + a^{-2/6}(\mathbf{I} - \mathbf{N}_r) \quad (9.3)$$

where

$$\mathbf{N}_r = \mathbf{n}_r \otimes \mathbf{n}_r \quad (9.4)$$

and \mathbf{n}_r is a fixed reference unit vector. We collect the relevant material in the following proposition.

Proposition 1. *Let \mathbf{B} and \mathbf{L} be in the set of symmetric and positive definite $n \times n$ matrices with determinant equal to d , denoted by \mathbb{P}_d , and consider the scalar function*

$$f(\mathbf{B}, \mathbf{L}) := \mathbf{B} \cdot \mathbf{L}^{-1} = \text{tr}(\mathbf{B}\mathbf{L}^{-1}).$$

Then, for every \mathbf{B} and \mathbf{L} in \mathbb{P}_d ,

$$f(\mathbf{B}, \mathbf{L}) \geq n, \quad \text{with equality only if } \mathbf{B} = \mathbf{L}, \quad (9.5)$$

so that

$$\min_{\mathbf{B} \in \mathbb{P}_d} f(\mathbf{B}, \mathbf{L}) = f(\mathbf{B}_0(\mathbf{L}), \mathbf{L}) = n, \quad \text{where } \mathbf{B}_0(\mathbf{L}) = \mathbf{L}. \quad (9.6)$$

Assume further that \mathbf{L} is of the form $\mathbf{L} = \mathbf{L}(\mathbf{R}) = \mathbf{R}\mathbf{L}_r\mathbf{R}^T$, where $\mathbf{R} \in \mathbb{R}ot$ is an arbitrary rotation and \mathbf{L}_r is (a constant matrix) of the form

$$\mathbf{L}_r = a^{\frac{2}{n}} \mathbf{n}_r \otimes \mathbf{n}_r + a^{-\frac{2}{(n-1)n}} (\mathbf{I} - \mathbf{n}_r \otimes \mathbf{n}_r) \quad (9.7)$$

with $a > 1$, \mathbf{n}_r a fixed unit vector, and \mathbf{I} the identity. Then

$$\begin{aligned} f_{\text{opt}}(\mathbf{B}) &:= \min_{\mathbf{R} \in \mathbb{R}ot} f(\mathbf{B}, \mathbf{R}\mathbf{L}_r\mathbf{R}^T) = f(\mathbf{B}, \mathbf{R}_0(\mathbf{B})\mathbf{L}_r\mathbf{R}_0^T(\mathbf{B})) = \\ &= a^{\frac{2}{(n-1)n}} \left[\text{tr}(\mathbf{B}) - (1 - a^{-\frac{2}{n-1}}) \lambda_{\max}^2(\mathbf{B}) \right] \end{aligned} \quad (9.8)$$

where the minimizer $\mathbf{R}_0(\mathbf{B})$ is a rotation that maps \mathbf{n}_r onto the eigenvector of \mathbf{B} corresponding to its largest eigenvalue $\lambda_{\max}^2(\mathbf{B})$. Finally,

$$\min_{\mathbf{B} \in \mathbb{P}_1} f_{\text{opt}}(\mathbf{B}) = n, \quad (9.9)$$

attained by any matrix $\mathbf{B} \in \mathbb{P}_1$ whose largest eigenvalue is $\lambda_{\max}^2(\mathbf{B}) = a^{2/n}$ and whose other eigenvalues are all equal to $a^{-2/(n-1)n}$.

Proof. Writing \mathbf{B} and \mathbf{L}^{-1} in spectral form we have

$$\begin{aligned} \mathbf{B} \cdot \mathbf{L}^{-1} &= \sum_{i=1}^n \lambda_i^2(\mathbf{B}) \mathbf{b}_i \otimes \mathbf{b}_i \cdot \sum_{j=1}^n \lambda_j^2(\mathbf{L}^{-1}) \mathbf{l}_j \otimes \mathbf{l}_j = \\ &= \sum_{i,j=1}^n \lambda_i^2(\mathbf{B}) \lambda_j^2(\mathbf{L}^{-1}) (\mathbf{b}_i \cdot \mathbf{l}_j)^2 \geq \sum_{i=1}^n \lambda_i^2(\mathbf{B}) \lambda_i^2(\mathbf{L}^{-1}) (\mathbf{b}_i \cdot \mathbf{l}_i)^2 \end{aligned}$$

with equality holding only if $(\mathbf{b}_i \cdot \mathbf{l}_j)^2 = 0$ for $i \neq j$, i.e., only if \mathbf{B} and \mathbf{L}^{-1} share their eigenspaces, in which case they commute. Since we want to minimize $\mathbf{B} \cdot \mathbf{L}^{-1}$, we restrict attention to this case in the rest of the proof.

Let $\mathbf{A} := \mathbf{B}\mathbf{L}^{-1}$. Since $\mathbf{B}, \mathbf{L} \in \mathbb{P}_d$ and $\mathbf{B}\mathbf{L}^{-1} = \mathbf{L}^{-1}\mathbf{B}$, then $\mathbf{A} \in \mathbb{P}_1$. Denoting by $\lambda_i^2(\mathbf{A})$ its eigenvalues, and using the well known inequality between arithmetic and geometric means, we have

$$\operatorname{tr}(\mathbf{A}) = \sum_{i=1}^n \lambda_i^2(\mathbf{A}) \geq n \left(\prod_{i=1}^n \lambda_i^2(\mathbf{A}) \right)^{\frac{1}{n}} = n (\det \mathbf{A})^{\frac{1}{n}} = n \quad (9.10)$$

where the inequality is always strict unless $\lambda_i^2(\mathbf{A}) = 1$ for all i , or $\mathbf{A} = \mathbf{I}$. This proves (9.5) and hence (9.6).

Observe now that

$$\mathbf{L}^{-1}(\mathbf{R}) = \mathbf{R}\mathbf{L}_r^{-1}\mathbf{R}^T, \quad \mathbf{L}_r^{-1} = a^{\frac{2}{(n-1)n}} \left[\mathbf{I} - (1 - a^{-\frac{2}{n-1}})\mathbf{n}_r \otimes \mathbf{n}_r \right], \quad (9.11)$$

and therefore

$$\mathbf{B} \cdot \mathbf{L}^{-1}(\mathbf{R}) = a^{\frac{2}{(n-1)n}} \left[\operatorname{tr}(\mathbf{B}) - (1 - a^{-\frac{2}{n-1}})\mathbf{B}\mathbf{R}\mathbf{n}_r \cdot \mathbf{R}\mathbf{n}_r \right]. \quad (9.12)$$

Since $1 - a^{-\frac{2}{n-1}} > 0$, this is minimized when $\mathbf{B}\mathbf{R}\mathbf{n}_r \cdot \mathbf{R}\mathbf{n}_r$ is maximal, i.e., when \mathbf{R} maps \mathbf{n}_r onto the eigenvector corresponding to the maximal eigenvalue $\lambda_{\max}^2(\mathbf{B})$ of \mathbf{B} . This establishes (9.8).

Finally, (9.9) follows by exchanging the order of minimization in \mathbf{B} and \mathbf{L} , in view of (9.6). We also give a more direct proof, which is instructive. To this end, we order the eigenvalues of \mathbf{B} so that $\lambda_n^2(\mathbf{B}) = \lambda_{\max}^2(\mathbf{B})$. Using again the inequality between arithmetic and geometric means, we have

$$\begin{aligned} \operatorname{tr}(\mathbf{B}) - (1 - a^{-\frac{2}{n-1}})\lambda_{\max}^2(\mathbf{B}) &= a^{-\frac{2}{n-1}}\lambda_{\max}^2(\mathbf{B}) + \sum_{i=1}^{n-1} \lambda_i^2(\mathbf{B}) \geq \\ &\geq n \left(a^{-\frac{2}{n-1}} \prod_{i=1}^n \lambda_i^2(\mathbf{B}) \right)^{\frac{1}{n}} = na^{-\frac{2}{(n-1)n}} \end{aligned}$$

with equality only if $a^{-\frac{2}{n-1}}\lambda_{\max}^2(\mathbf{B}) = \lambda_i^2(\mathbf{B})$, $i = 1, \dots, n-1$. Since $1 = \det \mathbf{B} = \lambda_{\max}^2(\mathbf{B})(\lambda_i^2(\mathbf{B}))^{(n-1)}$, this is possible if and only if $\lambda_{\max}^2(\mathbf{B}) = a^{\frac{1}{n}}$ and $\lambda_i^2(\mathbf{B}) = a^{-\frac{2}{(n-1)n}}$ for $i = 1, \dots, n-1$. This establishes (9.9) and completes the proof. \square

Acknowledgments

These lecture notes draw freely on work done in collaboration with P. Cesana, S. Conti, A. DiCarlo, G. Dolzmann, K. Urayama, and L. Teresi during the last ten years.

References

- [1] V. Agostiniani, A. DeSimone: Gamma-convergence of energies for nematic elastomers, forthcoming (2010).
- [2] J.S. Biggins, E.M. Terentjev, M. Warner: Semisoft elastic response of nematic elastomers to complex deformations, *Phys. Rev. E* **78**, 041704.1–9 (2008).
- [3] Bladon, P., Terentjev, E. M., Warner, M., 1993. Transitions and instabilities in liquid-crystal elastomers. *Phys. Rev. E* **47**, R3838–R3840.
- [4] P. Cesana, 2010. Relaxation of multi-well energies in linearized elasticity and applications to nematic elastomers. *Arch. Rat. Mech. Anal.*, in press.
- [5] P. Cesana, A. DeSimone, 2009. Strain-order coupling in nematic elastomers: equilibrium configurations. *Math. Models Methods Appl. Sci.* **19**, 601-630.
- [6] Conti, S., DeSimone, A., Dolzmann, G., 2002. Soft elastic response of stretched sheets of nematic elastomers: a numerical study. *J. Mech. Phys. Solids* **50**, 1431–1451.
- [7] Conti, S., DeSimone, A., Dolzmann, G., 2002. Semi-soft elasticity and director reorientation in stretched sheets of nematic elastomers. *Phys. Rev. E* **60**, 61710-1–8.
- [8] S. Conti, A. DeSimone, G. Dolzmann, S. Müller, F. Otto: *Multiscale modeling of materials: the role of analysis*. In: Kirkilionis, M., Krmker, S., Rannacher, R., Tomi, F. (eds.), *Trends in Nonlinear Analysis*, 375–408. Springer, Berlin Heidelberg New York (2002).
- [9] P.-G. de Gennes: *Weak nematic gels*. In: W. Helfrich and G. Heppke (eds.), *Liquid Crystals of One- and Two-dimensional Order*, 231–237. Springer, Berlin (1980).
- [10] P.-G. de Gennes, J. Prost *The Physics of Liquid Crystals* (Clarendon Press, Oxford 1993).
- [11] DeSimone, A., 1999. Energetics of fine domain structures. *Ferroelectrics* **222**, 275–284.
- [12] A. DeSimone, A. Di Carlo, L. Teresi, 2007. Critical volages and blocking stresses in nematic gels. *Eur. Phys. J. E* **24**, 303310.

- [13] DeSimone, A., Dolzmann, G., 2000. Material instabilities in nematic elastomers. *Physica D* 136, 175–191.
- [14] DeSimone, A., Dolzmann, G., 2002. Macroscopic response of nematic elastomers via relaxation of a class of $SO(3)$ -invariant energies. *Arch. Rat. Mech. Anal.* 161, 181–204.
- [15] A. DeSimone, L. Teresi, 2009. Elastic energies for nematic elastomers. *Eur. Phys. J. E* 29, 191204.
- [16] A. DeSimone, L. Teresi: Dynamic accessibility of low-energy configurations in nematic elastomers. In preparation (2010).
- [17] Finkelmann, H., Gleim, W., Kock, H.J., Rehage, G., 1985. Liquid crystalline polymer network - Rubber elastic material with exceptional properties. *Makromol. Chem. Suppl.* 12, 49.
- [18] Finkelmann, H., Kundler, I., Terentjev, E. M., Warner, M., 1997. Critical stripe-domain instability of nematic elastomers. *J. Phys. II France* 7, 1059–1069.
- [19] Finkelmann, H., Rehage, G., 1984. Liquid crystal side chain polymers. *Adv. Polymer Sci.* 60/61, 99.
- [20] A. Fukunaga, K. Urayama, T. Takigawa, A. DeSimone, L. Teresi: Dynamics of Electro-Opto-Mechanical Effects in Swollen Nematic Elastomers. *Macromolecules* 41, 9389–9396 (2008).
- [21] L. Golubović, T.C. Lubensky: Nonlinear elasticity of amorphous solids. *Phys. Rev. Lett.* 63, 1082–1085 (1989).
- [22] M.E. Gurtin, *Introduction to Continuum Mechanics*. Academic Press, New York 1981.
- [23] T. Ikeda, *Fundamentals of Piezoelectricity*. Oxford University Press, Oxford 1990.
- [24] Kundler, I., Finkelmann, H., 1995. Strain-induced director reorientation in nematic liquid single crystal elastomers. *Macromol. Rapid Comm.* 16, 679–686.
- [25] Martinoty, P., Stein, P., Finkelmann, H., Pleiner, H., Brand, H.R., 2004. Mechanical properties of monodomain side chain nematic elastomers, *Eur. Phys. J. E* 14, 311.

- [26] Menzel, A., Pleiner, H., Brand, H., 2009. Nonlinear relative rotations in liquid crystalline elastomers. *J. Chem. Phys.* 126, 234901-1-9.
- [27] D. Rogez, G. Francius, H. Finkelmann, P. Martinoty: Shear mechanical anisotropy of side chain liquid-crystal elastomers: Influence of sample preparation. *Eur. Phys. J. E* **20**, 369–378 (2006).
- [28] I. Stewart, *The static and dynamic continuum theory of liquid crystals* (Taylor Francis, London 2004).
- [29] Verwey, M. Warner, E. Terentjev: Elastic instability and stripe domains in liquid crystalline elastomers. *J. Phys. II France* **6**, 1273–1290 (1996).
- [30] M. Warner, E. M. Terentjev, *Liquid Crystal Elastomers*. Clarendon Press, Oxford 2003.
- [31] Weilepp, J., Brand, H., 1996. Director reorientation in nematic–liquid–single–crystal elastomers by external mechanical stress. *Europhys. Lett.* 34, 495–500.
- [32] F. Ye, R. Mukhopadhyay, O. Stenull, T.C. Lubensky: Semisoft nematic elastomers and nematics in crossed electric and magnetic fields, *Phys. Rev. Lett.* **98**, 147801 (2007).
- [33] Zubarev, E. R., Kuptsov, S. A., Yuranova, T. I., Talroze, R. V., Finkelmann, H., 1999. Monodomain liquid crystalline networks: reorientation mechanism from uniform to stripe domains. *Liquid Crystals* 26, 1531–1540.